
Site U1396¹

Expedition 340 Scientists²

Chapter contents

Background and objectives	1
Operations	1
Lithostratigraphy	2
Paleontology and biostratigraphy	4
Geochemistry	6
Physical properties	7
Paleomagnetism	8
References	9
Figures	11
Tables	27

Background and objectives

Integrated Ocean Drilling Program (IODP) Site U1396 (proposed Site CARI-01C; 16°30.49'N, 62°27.10'W; 801 meters below sea level [mbsl]) is the most western site drilled during Expedition 340 (Fig. F1).

The bathymetric survey for Site U1396 revealed a region bounded by a topographic high to the north and by two large canyons to the south. Site survey data indicated that this site could penetrate regular (unperturbed) seismic reflectors. The drill site is located on the topographic high to minimize any perturbations (e.g., related to turbidites). Site U1396 is located in the same area as the 5.75 m long CAR-MON 2 core taken during the *Caraval* cruise in 2002. Sediment recovered in the CAR-MON 2 core provides a stratigraphic record extending back ~250 k.y., as shown by $\delta^{18}\text{O}$ chronostratigraphy. The calculated sedimentation rate (including tephra) is ~2.3 cm/k.y. (Le Friant et al., 2008). The recovered core also contained material from several explosive Plinian eruptions, which had not previously been identified on land (Le Friant et al., 2008).

The objective for Site U1396 was to characterize the eruptive history of Montserrat. Volcanism started on Montserrat at ~2.6 Ma at Silver Hills and moved to Centre Hills between 0.5 and 1.0 Ma, with the youngest volcanism being centered on the Soufrière Hills–South Soufrière Hills complex (~170 ka to present) (Harford et al., 2002). With conventional coring it is only possible to retrieve samples of recent volcanic activity. Drilling to a target depth of 132 meters below seafloor (mbsf) at Site U1396 was intended to extend our knowledge of the volcanic history of Montserrat to the birth of the island at at least ~2.5 Ma. Petrologic, lithologic, sedimentologic, and geochronologic analyses of volcanic rocks and volcanoclastic material from this site are expected to date as far back as 4 Ma (assuming a sedimentation rate of 2.3 cm/k.y. from the CAR-MON 2 study) and will provide significant new constraints on the early development of volcanism on Montserrat and on the spatial and temporal distribution of volcanic activity.

Operations

Transit to Site U1396

After a 28.6 nmi transit from Site U1395 in cruise mode, the vessel arrived at Site U1396. The vessel stabilized over Site U1396 at

¹Expedition 340 Scientists, 2013. Site U1396. In Le Friant, A., Ishizuka, O., Stroncik, N.A., and the Expedition 340 Scientists, *Proc. IODP, 340*: Tokyo (Integrated Ocean Drilling Program Management International, Inc.).
doi:10.2204/iodp.proc.340.106.2013
²Expedition 340 Scientists' addresses.



2245 h on 16 March 2012. All times reported in this volume are given in ship local time, which was Universal Time Coordinated (UTC) – 4 h. The position reference was a combination of GPS signals and a single acoustic beacon. The positioning beacon was deployed at 2310 h on 16 March. At the end of operations at Site U1396, the beacon was sent an acoustic command to release. The beacon was retrieved at 0730 h on 18 March.

Site U1396

Site U1396 consists of three holes (Table T1). The original plan called for two holes to a depth of ~132 mbsf. The first hole was successfully cored and was terminated at a total depth of 134.9 mbsf. Hole U1396B was a short hole designed to capture an interval in Hole U1396A that was poorly recovered because of a shattered core liner. Hole U1396C was cored to a depth of 139.4 mbsf. No logging was scheduled at Site U1396. The advanced piston corer (APC) was deployed 31 times. The cored interval with the APC was 283.8 m with a recovery of 296.38 m of core (104%). Overall recovery for Site U1396 was 104%. There was one drilled interval of 5 m in Hole U1396B. Total time spent on Site U1396 was 34.75 h.

Hole U1396A

The vessel arrived at Site U1396 and was in position at 2245 h on 16 March 2012. After an uneventful pipe trip, the top drive was picked up and the bit was spaced out to spud Hole U1396A. The bit was initially set at 789 meters below rig floor (mbrf), and the core barrel was run in on wireline. The first attempt to recover the mudline came back without core. The bit was lowered to 795 mbrf for another attempt at a mudline core. The hole was spudded at 0345 h on 17 March. Seafloor depth was calculated from the length of the first core to be 798.9 mbrf (787.4 mbsl). Orientation was performed with the FlexIt tool on the first 12 cores with good results. Nonmagnetic core barrels were used for APC coring for Cores 340-U1396A-1H through 12H. There was only one coring anomaly during the hole; Core 2H had the liner shatter when the piston fired. Advanced piston corer temperature tool (APCT-3) measurements were taken on Cores 3H through 6H. There was only one partial stroke experienced in the entire piston coring sequence. A total of 15 piston cores were taken over a 134.9 m interval with a total recovery of 140.51 m of core (104%). After the completion of APC coring, the drill string was pulled back with the top drive still installed, and the bit cleared the seafloor at 1615 h on 17 March, ending Hole U1396A. The total time spent on Hole U1396A was 17.5 h.

Hole U1396B

After clearing the seafloor in Hole U1396A, the vessel was offset 20 m east and Hole U1396B was spudded at 1650 h on 17 March 2012. Seafloor depth was used from Hole U1396A, which was 798.9 mbrf (787.4 mbsl). The uppermost 5 m of Hole U1396B was drilled, and Core 340-U1396B-2H was shot from 5 mbsf. Both the FlexIt tool and nonmagnetic core barrels were used for Core 2H. One piston core was taken over the 9.5 m interval, with a total recovery of 10.00 m of core. Overall recovery for Hole U1396B was 105%. The hole was terminated after a single core, and the drill string was pulled clear of the seafloor at 1725 h. The total time spent on Hole U1396B was 1.25 h.

Hole U1396C

After clearing the seafloor in Hole U1396B, the vessel was offset 20 m south and Hole U1396C was spudded at 1810 h on 17 March 2012. Seafloor depth was calculated from the length of the first core 798.1 mbrf (786.6 mbsl). Orientation was performed with the FlexIt tool on all 15 cores with good results. Nonmagnetic core barrels were used all cores. APCT-3 measurements were taken on Cores 340-U1396C-6H and 11H. Microspheres were run on Cores 3H, 6H, and 14H. There was only one partial stroke in the entire piston coring sequence. Two of the cores (11H and 12H) had to be drilled over to release them from the formation. A total of 15 piston cores were taken over a 139.4 m interval with a total recovery of 145.92 m of core. Overall recovery for Hole U1396C was 105%. After the completion of APC coring, the top drive was set back and the drill string was pulled back to the rig floor. Drilling equipment was secured on the rig floor at 0935 h on 18 March, ending Site U1396 and Hole U1396C. The total time spent on Hole U1396C was 16.0 h. The vessel then proceeded underway to Site U1397.

Lithostratigraphy

Three holes were drilled at Site U1396. Holes U1396A and U1396C were drilled to 135.5 and 140.0 mbsf, respectively; Hole U1396B was only drilled to 15 mbsf. The aim of Hole U1396B was to fill out an interval of core that was poorly recovered (deformed during coring) in Hole U1396A.

This site mainly comprises a series of hemipelagic intervals and relatively thin (typically <10 cm and most often <5 cm) tephra layers in Units B and E. A distinctive very coarse grained unit rich in white felsic clasts (Unit D) provides a good marker horizon in Holes U1396A and U1396C. Massive volcanoclastic sand intervals comprise the remaining Units A and C.

Distinguishing fallout deposits from fine-grained distal turbidites

A key issue for the description of these deposits is to distinguish tephra layers deposited by fallout from eruption columns (“fallout deposits”) from distal turbidity current deposits. Both types of deposit can be normally graded and lack laminations. The criteria adopted for Expedition 340 are given below.

Fallout deposits contain very little or no reworked carbonate material. However, the amount of carbonate material is difficult to determine accurately by visual examination in fine-grained sediment. Therefore, a limited number of microscopic component analyses (as time on board permitted) were undertaken to determine composition. Importantly, fallout deposits tend to be better sorted than turbidites because of settling processes; turbidites tend to have very poor sorting. Only turbidites will display evidence of strong lateral flow, such as basal erosion and reworking as bed-load. However, basal erosion can be hard to determine unambiguously in narrow-diameter core barrels and can be overprinted by core deformation (downward bowing of basal contacts). Ripple cross-lamination will also only occur in turbidites, but it was rarely if ever seen in Site U1396 cores. Care needs to be taken to distinguish planar lamination due to tractional reworking (turbidites) from grain size and compositional zoning (tephra fallout).

Defining units

The lithostratigraphy of Site U1396, thick sequences of thin tephra layers and intervening hemipelagic units, does not lend itself to defining obvious lithostratigraphic units. Information from magnetic susceptibility curves should be considered in future studies to better constrain the stratigraphic record. For example, the cores contain hemipelagic intervals with increased sand content or variable color, which may be bioturbated tephra layers. The average accumulation rate of 3 cm/k.y. for Site U1396 means that thinner tephra layers are most likely reworked by burrowing organisms and seafloor currents.

Unit A

Depths: Hole U1396A = 0–0.4 mbsf, Hole U1396C = 0–0.4 mbsf

Unit A extends from 0 to 0.4 mbsf and comprises 39 cm of “soupy,” high-water content, bioclast-rich fine sand, which is only seen in Holes U1396A and U1396C (Hole U1396B did not sample the interval directly below the seafloor). This sand is massive and ungraded, and it could represent a high-density turbidite.

It seems likely that this unit is related to the 1995–recent eruption on Montserrat. The unit has an oxidized brown top and is unlikely to be an artifact of coring. A similar uppermost unit was not observed previously in other piston and gravity cores in the vicinity of Site U1396 (Le Friant et al., 2008; Cassidy et al., submitted).

Unit B

Depths: Hole U1396A = 0.4–116.1 mbsf, Hole U1396B = 5–14.5 mbsf, Hole U1396C = 0.4–116.1 mbsf

Unit B extends from 0.4 to 116.1 mbsf and comprises a thick sequence of interbedded hemipelagic mud and tephra layers, with the latter typically being <5 cm and rarely >10 cm in thickness. In general, hemipelagic mud makes up most of Unit B. Tephra layers become more common below 90–95 mbsf, as seen in the magnetic susceptibility data. Hemipelagic mud dominates the middle part of the unit.

Thin black or brown fine sand and silt layers (typically <5 cm thick) are common in Unit B and most likely represent fallout deposits. In some cases their coarse grain size (and well-sorted nature) and exclusively volcanoclastic composition is strong evidence for fallout. There may be many more cryptotephra, which are not visible upon visual examination, within the hemipelagic mud intervals.

Most cores at this site comprise hemipelagic mud and thin tephra, with the only exceptions being a few thick tephra layers that are described in more detail below.

Thick tephra layers

Tephra units thicker than 12 cm are observed in only a few instances:

- Upper 5 m: the uppermost part of Unit B (only seen in Hole U1396A) has two thick (20–30 cm) poorly sorted sand layers with a mixed bioclastic (20%–50%) and volcanoclastic (50%–80%) composition at 1.7 and 2.6 mbsf. These mixed composition units are most likely turbidites. Sandwiched within the lower unit is a well-sorted layer comprising 99% volcanic material that is a few centimeters thick and is most likely a fallout unit. Together with a 4 cm (fallout) tephra layer at 3.7 mbsf, these tephra layers occur within the uppermost 5.7 mbsf. Similarly thick tephra layers are not apparent in the 5.7 m long CAR-MON 2 core studied by Le Friant et al. (2008) that extends to 250 ka, suggesting these thick tephra have a localized distribution. The CAR-MON 2 core was located ~15 km from Site U1396, nearer to Montserrat on the same bathymetric ridge. The two

thick sand layers seen in the upper 5.7 m of Hole U1396A may be correlative to the more subtle cryptotephra described by Le Friant et al. (2008).

- Two 12–15 cm mixed bioclastic-volcaniclastic poorly sorted turbidites occur in Hole U1396C at 11.2 and 10.2 mbsf.
- A ~50 cm well-sorted coarse fallout unit occurs at 34.3 mbsf in Hole U1396A and comprises at least two graded sequences.
- A 24 cm thick dark coarse tephra layer occurs at 48.7 mbsf in Hole U1396C.
- A 22 cm thick well-sorted fallout deposit occurs at 82.7 mbsf in Hole U1396A and may be equivalent to a 14 cm layer at 78.5 mbsf in Hole U1396C or a 35 cm thick layer at 84.4 mbsf in Hole U1396C.
- Three coarser units occur near the base of the unit in Hole U1396A. A distinctive 50 cm thick, dark gray, massive, poorly sorted medium sand occurs at 106.7 mbsf and is most likely a volcaniclastic turbidite.
- In Hole U1396A a 12 cm thick, coarse, well-sorted fallout unit occurs at 111.4 mbsf, and a 35 cm thick well-sorted fallout deposit occurs at 115.2 mbsf.

Isolated pebble-sized volcanic clasts

Individual outsize volcanic clasts (≤ 1 cm) are observed in the hemipelagic mud in a few locations. Their origin (perhaps as reworked dropstones) is poorly understood at present.

Inclined laminated sandstone

A 14 cm interval of fine to medium sand is seen in Hole U1396C at 110.7 mbsf; the interval has inclined and truncated laminations that are enigmatic.

Unit C

Depths: Hole U1396A = 116.1–122 mbsf, Hole U1396C = 116.1–122 mbsf

Unit C extends from 116.1 to 122 mbsf in Holes U1396A and U1396C and comprises massive medium-coarse volcaniclastic sand. The sand has ~85% light-colored andesitic lava grains within a finer darker matrix made mainly of mineral crystals. The sand hue changes progressively vertically, and these changes in hue represent compositional zoning. Unit C is darker than the overlying and underlying units and has some dispersed 1 cm clasts near its base. Unit C may represent high-density turbidity current deposition.

Unit C is absent or poorly developed in Hole U1396A and was too deep for Hole U1396B. Preliminary comparison of the core logs does not indicate

an obvious correlative unit in Hole U1396A at a similar depth below seafloor. If Unit C does not represent sand sucked in during APC coring (i.e., it is not an artifact of drilling), this is surprising, as Holes U1396A and U1396C are separated by just 28 m.

Unit D

Depths: Hole U1396A = 122–123.9 mbsf, Hole U1396C = 122–123.9 mbsf

Unit D extends from 122 to 123.9 mbsf. This unit comprises a distinctive series of unusually coarse (commonly as large as centimeter-scale clasts) breccias with a pinkish color (Fig. F2). Five stacked fining-upward units make up Unit D in Holes U1396A and U1396C, with the uppermost unit being the thickest. The uppermost unit has very well sorted intervals of pebble-sized (≤ 2 cm) material, with little or no sand or mud-sized matrix material. These normally graded intervals are 3–62 cm thick and separated by thin (1–5 cm) layers of massive fine sand or silt. Unit D is similar in thickness and grading in Holes U1396A and U1396C. The similar stratigraphy beneath Unit D in both holes suggests it has not eroded underlying strata, which is consistent with air fall deposition.

Unit E

Depths: Hole U1396A = 123.9–135.5 (bottom of hole), Hole U1396C = 123.9–140 mbsf (bottom of hole)

Unit E extends from 123.9 mbsf to the base of Hole U1396C at 140 mbsf. This unit comprises hemipelagic mud and relatively abundant thin (< 10 cm) tephra layers. Many of these tephra layers are well-sorted and this is consistent with fallout deposition.

Paleontology and biostratigraphy

Core catcher samples at Site U1396 contain calcareous nannofossils and planktonic and benthic foraminifers of varying abundances and at varying levels of preservation. Preservation deteriorates with depth; however, it remains adequate for confident biostratigraphic age assignment. Both nannofossil and planktonic foraminiferal biostratigraphic data and magnetostratigraphic dates for Site U1396 indicate ages ranging from late Pleistocene to early Pliocene (Fig. F3). Sedimentation rate appears to increase with depth (see “**Paleomagnetism**” for further discussion). Sponge spicules and ostracods are scarce and generally moderately preserved. Pteropods and heteropods were not found in any core catcher samples.

Calcareous nannofossils

Nannofossil preservation was good to moderate throughout the 13 core catcher samples analyzed from Hole U1396A (of 15 collected), one sample from Hole U1396B, and 13 samples from Hole U1396C (of 15 collected). The remaining core catcher samples were not analyzed because of the coarse nature of the material collected.

Sample 340-U1396A-1H-CC contains abundant *Gephyrocapsa caribbeanica*, common *Helicosphaera hyalina*, and small forms (2.5–3 µm) that may be *Emiliania huxleyi*. The presence of *E. huxleyi* was further substantiated by the absence of *Pseudoemiliana lacunosa*. Thus, this sample lies within the *E. huxleyi* Zone (Zone CN15; Okada and Bukry, 1980). The age of this sample is younger than 0.25 Ma (Kameo and Bralower, 2000).

Samples 340-U1396A-2H-CC to 4H-CC yielded a variety of small *Gephyrocapsa* species, *P. lacunosa*, and *Crenolithus doronicoides*. The latter species defines Zone CN13 (Okada and Bukry, 1980). *G. caribbeanica* is abundant throughout these three core catcher samples; therefore, these samples are within Subzone CN13b (Okada and Bukry, 1980). Moreover, *Calcidiscus macintyreii* is common in Sample 340-U1396A-4H-CC. Gartner (1977) has used this species to divide the Quaternary. Herein, Gartner's methodology has been followed using the revised zonation for this sample. Sample 340-U1396A-4H-CC lies within Subzone CN13b (Okada and Bukry, 1980) or the *C. macintyreii* Zone (Gartner, 1977). Overall preservation is good to moderate.

Sample 340-U1396A-5H-CC yielded a characteristic Pliocene assemblage with abundant *Discoaster brouweri* and common *C. macintyreii*. The *D. brouweri* are extremely affected by overgrowth; however, identification was possible. Otherwise, the sample contained abundant specimens with good preservation. *C. macintyreii* and *D. brouweri* are indicative of an upper Pliocene assemblage, placing this sample within Subzone CN12d. Sample 340-U1396A-6H-CC contains an abundant and well-preserved Pliocene assemblage with *Discoaster surculus*, *D. brouweri*, *C. macintyreii*, and *Hayaster perplexus*. Generally, *Discoaster* species were well preserved in comparison to Sample 340-U1396A-5H-CC. Because of the absence of *Discoaster tamalis*, Sample 340-U1396A-6H-CC was placed within Subzone CN12b (Okada and Bukry, 1980). Samples 340-U1396A-7H-CC to 10H-CC yielded a characteristic lower Pliocene assemblage with a variety of *Discoaster* species. *D. pentaradiatus*, *D. surculus*, *D. brouweri*, *Discoaster asymmetricus*, and *D. tamalis* are common. *Discoaster variabilis* and *Discoaster challengerii* are generally less abundant (few to none). The preservation, especially of *Discoaster* specimens, in

this sample is good except for *Ceratolithus rugosus*, which is heavily overgrown, destroying the general morphology. Because neither *Sphenolithus abies/neoabies* nor *Reticulofenestra pseudoumbilica* were detected, this sample was assigned to Subzone CN12a.

Samples 340-U1396A-11H-CC to 15H-CC contain *S. abies/neoabies* and *R. pseudoumbilica*, which indicate lower Pliocene Subzone CN11a.

In Hole U1396B, zones, subzones, and ages similar to those in Hole U1396A were identified. The top core catcher samples are placed in the Quaternary, whereas the bottom samples (340-U1396B-6H-CC to 15H-CC) show trends similar to those in Hole U1396A, indicating an age of late to early Pliocene. Hole U1396B recovered only one core catcher sample (340-U1396B-2H-CC), which yielded an upper Pleistocene assemblage with *G. caribbeanica*, *G. oceanica*, and *H. hyalina*. Sample 340-U1396B-2H-CC was assigned to Subzone CN14a (Okada and Bukry, 1980).

Planktonic foraminifers

All 31 core catcher samples from Site U1396 were analyzed for foraminiferal content. Only two samples, 340-U1396C-1H-CC and 2H-CC, did not suggest a reliable age because they lacked marker taxa. Three samples, 340-U1396A-12H-CC and 13H-CC and 340-U1396C-13H-CC, had extremely low foraminiferal content because of an influx of volcanic material. Samples 340-U1396A-13H-CC and 340-U1396C-13H-CC can still, however, be dated to the *Sphaeroidinellopsis seminulina* Zone (PL3), as they contain *S. seminulina*. Species abundances in the Pleistocene generally conform to the previous sites (U1394 and U1395), with *Globigerinoides ruber* and *Globigerinoides sacculifer* being the two most dominant species. Throughout the Pliocene these abundances shift, with a distinct increase in the keeled genus *Globorotalia* (specifically: *Globorotalia exilis*, *Globorotalia pertenuis*, *Globorotalia menardii*, and *Globorotalia miocenica*) becoming more common.

Every planktonic foraminiferal biozone and subzone from the Quaternary to the lower Pliocene was recorded (Zones PT1b, PT1a, PL6, PL5, PL4, PL3, PL2, and PL1). Several differences exist between the two main holes, U1396A and U1396C. Hole U1396A does not appear to capture the 30,000 y long Zone PL4 (*Dentoglobigerina altispira* Highest Occurrence Zone [HOZ]), although it was identified in Hole U1396C. Postcruise analysis of Hole U1396A may still identify this zone, likely within Core 340-U1396A-10H. Additionally, Zone PL1 (*Globorotalia tumida*/*Globoturborotalia nepenthes* Concurrent Range Zone (CRZ) [Atlantic]) was identified at the base of Hole U1396A (Sample 340-U1396A-15H-CC) but not in Hole U1396C. Again, further analysis of Core 340-

U1396C-15H may reveal the presence of *G. nepenthes*, which would indicate Zone PL1. Core catcher Sample 340-U1396C-3H-CC contains both *Globorotalia tosaensis* and *Globorotalia flexuosa*, which have conflicting and nonconcurrent ranges. The missing 21,000 y interval between when *G. flexuosa* goes extinct and *G. tosaensis* originates appears to have been the victim of time averaging, either through bioturbation, drilling, or some other mechanism. The primary marker between Subzone PT1a and Zone PL6 (*Globigerinoides fistulosus*) was not recorded at the expected depth, above the base of *Globorotalia truncatulinoidea*. *G. fistulosus* was recorded in only three samples (340-U1396A-3H-CC and 340-U1396C-5H-CC and 6H-CC). Zone PL6 was recognized, instead, on the base of *G. truncatulinoidea*, the first secondary datum within Zone PL6. Many different datums were recorded: *G. flexuosa* (0.07–0.40 Ma), *G. tosaensis* (top occurrence [T] at 0.61 Ma), *G. exilis* (T 2.1 Ma), *Globigerinoides extremus* (T 2.1 Ma), *G. miocenica* (T 2.39 Ma), *G. pertenuis* (T 2.60 Ma), *Globorotalia multicamerata* (T 2.99 Ma), *S. seminulina* (T 3.16 Ma), *Pulleniatina primalis* (T 3.65 Ma), *Globorotalia margaritae* (T 3.84 Ma), and *G. nepenthes* (T 4.36 Ma). Although several more first appearance datums (B) are calibrated through this interval as secondary markers, when compared against the datums listed above they appear to be largely unreliable as age determinations at this site and were not used.

Benthic foraminifers

A total of 41 genera and 44 species were identified at Site U1396 in the >150 μm size fraction. Benthic foraminifers examined in Holes U1396A, U1396B, and U1396C varied in abundance, diversity, and preservation (moderate). Hole U1396A has the greatest number of species (40), followed by Hole U1396B (25) and then Hole U1396C (4). Rotaliids have low diversity and are present in low abundances (1–10 specimens per sample) overall in Holes U1396A and U1396C. *Cibicides* and *Cibicidoides* are the dominant genera in Hole U1396A but are nearly absent in Holes U1396B and U1396C. *Cibicides wuellerstorfi* is the most abundant species in Hole U1396A. Similarly, buliminids have low diversity with low abundances (1–10 specimens per sample) overall in Holes U1396A and U1396C. However, buliminids dominate the assemblage in Samples 340-U1396A-4H-CC, 5H-CC, 8H-CC, and 9H-CC and 340-U1396C-3H-CC, 4H-CC, and 8H-CC. Miliolids are practically absent in most samples, with the exception of *Pyrgo murrhina*, the dominant species. Agglutinated foraminifers are represented by the genera *Sigmoilopsis*, *Bigenerina*, and *Vulvulina*, with *Karreriella bradyi* as the dominant species. Benthic foraminiferal density is generally low at Site U1396, ranging between 1 and 67 foraminifers/g of sediment.

However, Samples 340-U1396A-5H-CC and 10H-CC and 340-U1396C-4H-CC and 13H-CC have densities of 214, 111, 156, and 113 foraminifers/g of sediment, respectively.

At Site U1396, *Mylostomella costai*, *Mylostomella huygaensis*, *Orthomorphina jedlitschkai*, *Orthomorphina perversa*, *Pleurostomella alternans*, *Proxifrons inaequalis*, *Siphonodosaria cooperensis*, *Siphonodosaria insecta*, *Siphonodosaria pomuligera*, *Siphonodosaria sargrinensis*, *Stilostomella fistuca*, and *Vulvulina pennatula* are present in relative low abundances (1–10 specimens per sample) in most samples. This group has a last appearance datum (T) at 0.58 Ma (Hayward et al., 2006). *S. cooperensis* has a moderate abundance (1–30 specimens per sample) in Samples 340-U1396A-4H-CC, 5H-CC, and 6H-CC. Based on the presence and persistence of the above group, a bathyal paleodepth is interpreted.

Geochemistry

Samples for headspace analyses were taken from 15 depths throughout Hole U1396A. The uppermost sample (from Section 340-U1396A-1H-3) has a methane concentration of 3.6 ppm, but all other samples have levels between 2.1 and 2.6 ppm. No higher hydrocarbons were detected.

A total of 30 samples were taken for X-ray diffraction (XRD) and carbonate analysis. No pure volcanic samples were collected from Hole U1396A. In contrast to the previous sites, high Mg-calcite was only present in one section (340-U1396A-6H-2). All other carbonate-rich layers contain pure calcite and aragonite in variable proportions, with calcite generally dominant. Clay minerals are ubiquitous throughout the hole, with smectite and kaolinite present in all samples and glauconite commonly identified (e.g., Section 340-U1396A-9H-2; Fig. F4A). Halloysite may be present in some samples, but the spectra are not clear enough to be certain. The bulge beneath the main peaks in some of the volcanic-rich samples (e.g., Section 340-U1396A-12H-5; Fig. F4B) suggests that significant amounts of volcanic glass are present in some tephra layers.

CaCO_3 and organic carbon abundances reflect mixtures of carbonate-rich hemipelagic sediments with carbonate-free and organic carbon-free volcanogenic material delivered by ash fallout. The highest CaCO_3 concentration was only 72 wt%, with most samples having much lower levels, suggesting that volcanic material is dispersed throughout the core even where it is not visible to the naked eye (Fig. F5; Table T2).

Samples for pore water extraction were taken from every core from Hole U1396C (Fig. F6; Table T3). Alkalinity values are generally low (<1.5 mM) throughout the hole (Fig. F6A). pH values are generally lower

(7.6–7.1) than those at Sites U1394 and U1395, but no consistent pattern is observable in the data. Ammonia concentrations are much lower than those at the previous two sites (Fig. F6B). These differences may be related to the fact that Site U1396 is located at shallow depths on a basement high, where strong bottom currents have been observed on previous research cruises to the area. This effect tends to winnow out the finer grained, more reactive organic matter and leads to less intense organic carbon-driven diagenesis. Calcium concentrations are consistently higher than bottom water values in samples from throughout the hole (Fig. F6C), and magnesium concentrations are consistently lower than seawater concentrations (Fig. F6D). These features are commonly seen in deep sediment pore water as a result of alteration of basaltic glass and suggest that many of the tephra layers observed in the core may have a basaltic composition. This hypothesis is supported by the potassium concentrations which are also lower than seawater (Fig. F6E). Overall, ΣS concentrations are slightly depleted relative to seawater sulfate values but do not show a particularly distinct trend with depth. Chloride concentrations fluctuate within the normal range (550–570 mM) expected for pore water obtained from squeezing carbonate-rich sediment (Table T3).

Three samples were taken for shore-based microbiological analyses after the piston core had been preloaded with a microsphere bag to assess potential surface contamination. However, the bag failed to burst at the bottom of the hole. A total of 20 g of sediment was taken for shore-based microbiological activity measurements and stored at 0°C. A total of 4 g of sediment was taken for shore-based RNA analysis and stored at –80°C.

Physical properties

We collected physical properties data between 0 and 140 mbsf at Holes U1396A and U1396C. We also collected physical properties data between ~5 and 15 mbsf at Hole U1396B to fill a gap in the data from Hole U1396A. Good correlation exists between holes. Magnetic susceptibility provides the most valuable tool for differentiating stratigraphic changes at this site. *P*-wave and density measurements are consistent but show little variability with depth. Porosity measurements in sandy sediment are anomalously high, possibly an artifact of the core recovery process. All shear strength measurements increase monotonically with depth, with a few anomalous values. Temperature increases linearly with depth, with a temperature gradient of $69.3^\circ \pm 1.5^\circ\text{C}/\text{km}$. There is no evidence for fluid advection disturbing the temperature measurements.

Stratigraphic correlation between Holes U1396A and U1396C

We used magnetic susceptibility to correlate depths between Holes U1396A, U1396B, and U1396C (Figs. F7, F8). Hole U1396C is the reference hole for these correlations because it has the longest continuous record. Core 340-U1396A-2H shattered during coring, and although much of the sediment from the core was recovered, placed into core barrels on deck, and scanned on the Whole-Round Multisensor Logger (WRMSL), there is a chance that a significant amount of the material was disturbed during this process. We therefore removed all WRMSL data for Core 340-U1396A-2H from the correlation analysis. Core 340-U1396B-2H covers most of the depth range missing from Hole U1396A for correlation. By correlating both Holes U1396A and U1396B to Hole U1396C, we were able to make a nearly complete correlation at Site U1396. Core 340-U1396B-1H had all depth values set to 5 mbsf when we downloaded the data (this has since been changed); therefore, we applied a linear interpolation for Core 340-U1396B-1H to correlate this upper core with Hole U1396C. Holes U1396A and U1396B correlate well with Hole U1396C, with correlation coefficients of 0.75 and 0.79, respectively (Figs. F7, F8). Depth shifts for all correlation corrections for Holes U1396A and U1396B never exceeded 3 m and rarely exceeded 1 m. In the uppermost 7 m, we see clear correlation of turbidite units between the two holes. All correlation pick depth shifts are shown in Tables T4 and T5.

Gamma ray attenuation density, magnetic susceptibility, and *P*-wave velocity

Magnetic susceptibility identifies volcanoclastic layers embedded in the hemipelagic background. Natural gamma radiation (NGR) shows low-amplitude and low-frequency variations with depth on a wavelength of one to two core lengths. NGR values are generally anticorrelated with magnetic susceptibility anomalies. Gamma ray attenuation (GRA) density does not have any systematic trend or correlation with volcanoclastic layers.

Thermal conductivity

Thermal conductivity was measured on 50 sections. The mean value was 1.041 W/(m·K) with a standard deviation of 0.079 W/(m·K) and a standard error of the mean of 0.010 W/(m·K).

Shear strength

Handheld penetrometer measurements of undrained shear strength (S_u) in Holes U1396A and U1396C are consistent and show a general trend that increases

downhole. No measurements were performed in Hole U1396B. S_u measurements conducted with the automated vane shear (AVS) also show a trend of increasing shear strength with depth in both holes. Within this trend, a few low values are observed at 85, 115, and 130 mbsf.

P-wave velocities

Discrete measurements of *P*-wave velocity measured on the *x*-axis (PW-X) identify the volcanoclastic layers as having high velocity (1650–1800 m/s) compared to the hemipelagic sediment (1550–1650 m/s). Such measurements were only possible where tephra layers were thicker than the transducer's caliper separation (3 cm). PW-X measurements generally match *P*-wave logger (PWL) measurements on the WRMSL.

Moisture and density

We collected 35 moisture and density (MAD) samples (32 from Hole U1396A and 3 from Hole U1396C; Figs. F9, F10). Porosity ranges from ~54% to 70%, with one volcanic sand sample having a porosity of 50%. Porosity shows no clear trend with depth. We caution that our calculated porosity values in high-permeability sediments such as volcanic turbidites may be too low because many of the samples drained water when we removed them from the working half of the split core. When we baked these samples, less water was present for removal, resulting in porosities that will be systematically lower than true values. Normally compacted sands do not typically have porosities >50%. The deepest sediments at Site U1396 are ~4.5 Ma in age and sedimentation rates are low (see “Paleomagnetism”), implying that no significant overpressure or anomalously high porosities should exist at this site. We therefore suggest that the anomalously high porosities we observe in sandy sediment at Site U1396 may result from significant reworking of the sediment during core recovery and splitting. Bulk density ranges from 1.45 to 2.00 g/cm³. Grain density ranges between 2.65 and 2.8 g/cm³.

Downhole temperature

Temperature was measured with the APCT-3 at the bottom of Cores 340-U1396A-3H, 4H, 5H, and 6H (24.6, 34.1, 43.6, and 53.1 mbsf, respectively) and Cores 340-U1396C-6H and 11H (55.9 and 103.4 mbsf, respectively). Downhole temperature was monitored for 320, 316, 346, 654, 943, and 2281 s, respectively. Temperature was calculated from these time series of temperature measurements using TP-Fit (see APCT-3 user manual on the Cumulus/Techdoc database at iodp.tamu.edu/tasapps/). We assume a thermal con-

ductivity (*k*) of 1.0 W/(m·K) and $\rho C = 3.7 \times 10^6$ J/m³K. To calculate uncertainty, we assume *k* ranges from 0.9 to 1.1 W/(m·K) and ρC is between 3.2×10^6 and 4.0×10^6 J/m³K. At the base of Cores 340-U1396A-3H, 4H, 5H, and 6H we obtained temperatures of $7.62^\circ \pm 0.02^\circ\text{C}$, $8.33^\circ \pm 0.02^\circ\text{C}$, $8.79^\circ \pm 0.02^\circ\text{C}$, and $9.64^\circ \pm 0.02^\circ\text{C}$, respectively. At the base of Cores 340-U1396C-6H and 11H we obtained temperatures of $9.87^\circ \pm 0.02^\circ\text{C}$ and $13.07^\circ \pm 0.01^\circ\text{C}$, respectively. We have no reliable measure of the temperature of ocean water at the seafloor. Computed uncertainties are similar to the error on the best-fit solution and the probe's measurement accuracy.

A best-fit linear relationship between depth and our six temperature measurements gives a temperature gradient of $69.3^\circ \pm 1.5^\circ\text{C}/\text{km}$ (Fig. F10). Using measured thermal conductivity, the implied heat flow, if conductive, is 72 ± 2 mW/m². The near-surface heat flow at this site is reduced by 2% owing to the bathymetry, and sedimentation has a negligible effect on heat flow (Manga et al., 2012). There is no statistically significant deviation of the measurements from a straight line, and hence there is no signature of fluid flow in the temperature measurements (Manga et al., 2012).

Paleomagnetism

Cores 340-U1396A-1H through 12H, 340-U1396B-2H, and 340-U1396C-1H through 15H were recovered using nonmagnetic core barrels with the APC. All other APC cores were recovered using standard steel barrels. The FlexIt orientation tool was used on all APC cores recovered with nonmagnetic barrels; thus, declination for 0–107.4 mbsf in Hole U1396A, 5–15 mbsf in Hole U1396B, and 0–139.5 mbsf in Hole U1396C can be corrected to true north. Where FlexIt tool data were not available in Hole U1396A, declination was guided by the discrete inclination data (see “Paleomagnetism” in the “Methods” chapter [Expedition 340 Scientists, 2013]). Expected inclination for the site is 30.7° during normal polarity and -30.7° during reversed polarity, assuming a geocentric axial dipole (GAD). The archive halves of cores from Holes U1396A, U1396B, and U1396C were measured on the three-axis superconducting rock magnetometer (SRM) at 2.5 cm intervals (Table T6). Natural remanent magnetization (NRM) was measured before (NRM₀) and after stepwise alternating field demagnetization at 10 mT (NRM₁₀) and 20 mT (NRM₂₀). Core 340-U1396B-2H was substituted into the Hole U1396A record using magnetic susceptibility correlations (see “Physical properties”) because Core 340-U1396A-2H was highly disturbed after the core liner shattered. Eighteen discrete samples were

collected from the center of the working half of the core to compare to the SRM data (see “**Paleomagnetism**” in the “Methods” chapter [Expedition 340 Scientists, 2013]).

Cores are dominated by hemipelagic sediment but also contain many centimeter-scale fine-grained tephra layers from numerous eruptions of the Lesser Antillies volcanic arc (see “**Lithostratigraphy**”).

Results

NRM₀ (red) and NRM₂₀ (blue) intensities are shown for Holes U1396A and U1396B in Figure F11 and Hole U1396C in Figure F12. NRM₀ intensity is relatively high at ~0.5 m/A. Discrete tephra layers produce a strong magnetic susceptibility response (see “**Physical properties**”), and similarly high values of NRM₀ related to the concentration of ferrimagnetic minerals.

A strong magnetic overprint characterized by a steep SRM inclination and divergence of SRM and discrete inclination data is restricted to Cores 340-U1396A-13H through 15H. These cores were recovered using steel barrels. Agreement of SRM and discrete declination values from these cores suggests the radial overprint is less affected than the vertical overprint and declination can still be used for interpretation of polarity.

Magnetostratigraphy

Sedimentation rates for the site were predicted to be ~2–3 cm/k.y. from analysis of a 6 m gravity core (Le Friant et al., 2008). Extrapolation of these rates over the full 140 m record of Hole U1396C suggests the site could contain a 4–5 m.y. record of sedimentation. Inclination and declination for Holes U1396A, U1396B, and U1396C are shown in Figures F11 and F12. The Hole U1396A/U1396B record contains fifteen 180° shifts in declination in which declination stabilized before again reversing. The Hole U1396C record contains sixteen such reversal horizons. Changes in inclination are coeval with declination changes moving between positive and negative GAD values during these events. However, as only a 60° transition marks an inclination reversal, some of the shorter features that are clear in 180° declination shifts are not as obvious in inclination.

Using magnetic susceptibility to correlate between Holes U1396A, U1396B, and U1396C (see “**Physical properties**”), Holes U1396A and U1396B was transferred onto the more complete and longer depth scale of Hole U1396C to provide an aggregated reversal record (Fig. F13). This transfer also allowed more accurate splicing of the Hole U1396B record into the Hole U1396A record. This record is now referred to

as Hole U1396A/B. On a common depth scale the two declination records agree very well and suggest that the geomagnetic field was accurately recorded in the sediment at Site U1396.

Using the geomagnetic polarity timescale (GPTS) of Cande and Kent (1995), eight periods of normal polarity and nine periods of reversed polarity were determined in Hole U1396A/B and nine normal polarity and nine reversed polarity episodes in Hole U1396C. The earliest polarity reversal in Hole U1396A is the beginning of Chron C3n.1n (4.29 Ma) at 129.4 mbsf, giving Hole U1396A a basal age of 4.29–4.48 Ma. The longer Hole U1396C record contains the end of Chron C3n.2n (4.48 Ma), giving the hole a basal age of 4.48–4.62 Ma. These ages are in excellent agreement with nannofossil and foraminiferal ages, which put the base of both holes within the early Pliocene (Fig. F14; see “**Paleontology and biostratigraphy**”).

Using the depths of the dated reversals, an age-depth relationship can be created and sedimentation rates calculated for the longer record from Hole U1396C (Fig. F14). A linear sedimentation rate calculated from the deepest reversal gives the core an average sedimentation rate of 3.1 cm/k.y. However, this gradient steepens with depth in all three stratigraphic proxies. Pliocene sedimentation rates are double (4 cm/k.y.) the Pleistocene rates (1.7 cm/k.y.), and rates within the earliest 1 m.y. of the record from the base of the core to the beginning of the Gauss Chron (3.58 Ma) are even higher ~5.3 cm/k.y.

References

- Cande, S.C., and Kent, D.V., 1995. Revised calibration of the geomagnetic polarity timescale for the Late Cretaceous and Cenozoic. *J. Geophys. Res., [Solid Earth]*, 100(B4):6093–6095. doi:10.1029/94JB03098
- Cassidy, M., Trofimovs, J., Palmer, M.R., Talling, P.J., Watt, S.E.L., Moreton, S.G., and Taylor, R.N., submitted. Timing and emplacement dynamics of newly recognized mass flow deposits at ~8–12 ka offshore Soufrière Hills Volcano, Montserrat: how submarine stratigraphy can complement subaerial eruption histories. *J. Volcanol. Geotherm. Res.*
- Expedition 340 Scientists, 2013. Methods. In Le Friant, A., Ishizuka, O., Stroncik, N.A., and the Expedition 340 Scientists, *Proc. IODP, 340*: Tokyo (Integrated Ocean Drilling Program Management International, Inc.). doi:10.2204/iodp.proc.340.102.2013
- Gartner, S., 1977. Calcareous nannofossil biostratigraphy and revised zonation of the Pleistocene. *Mar. Micropaleontol.*, 2:1–25. doi:10.1016/0377-8398(77)90002-0
- Harford, C.L., Pringle, M.S., Sparks, R.S.J., and Young, S.R., 2002. The volcanic evolution of Montserrat using ⁴⁰Ar/³⁹Ar geochronology. *Mem.—Geol. Soc. London*, 21:93–113. doi:10.1144/GSL.MEM.2002.021.01.05

- Hayward, B.W., Kawagata, S., Grenfell, H.R., Droxler, A.W., and Shearer, M., 2006. Mid-Pleistocene extinction of bathyal benthic foraminifera in the Caribbean Sea. *Micropaleontology*, 52(3):245–265. doi:10.2113/gsmicro-pal.52.3.245
- Kameo, K., and Bralower, T.J., 2000. Neogene calcareous nannofossil biostratigraphy of Sites 998, 999, and 1000, Caribbean Sea. In Leckie, R.M., Sigurdsson, H., Acton, G.D., and Draper, G. (Eds.), *Proc. ODP, Sci. Results*, 165: College Station, TX (Ocean Drilling Program), 3–17. doi:10.2973/odp.proc.sr.165.012.2000
- Le Friant, A., Lock, E.J., Hart, M.B., Boudon, G., Sparks, R.S.J., Leng, M.J., Smart, C.W., Komorowski, J.C., Depilus, C., and Fisher, J.K., 2008. Late Pleistocene tephrochronology of marine sediments adjacent to Montserrat, Lesser Antilles volcanic arc. *J. Geol. Soc. (London, U. K.)*, 165(1):279–289. doi:10.1144/0016-76492007-019
- Manga, M., Hornbach, M.J., Le Friant, A., Ishizuka, O., Stroncik, N., Adachi, T., Aljahdali, M., Boudon, G., Breitzkreuz, C., Fraass, A., Fujinawa, A., Hatfield, R., Jutzeler, M., Kataoka, K., Lafuerza, S., Maeno, F., Martinez-Colon, M., McCanta, M., Morgan, S., Palmer, M.R., Saito, T., Slagle, A., Stinton, A.J., Subramanyam, K.S.V., Tamura, Y., Talling, P.J., Villemant, B., Wall-Palmer, D., and Wang, F., 2012. Heat flow in the Lesser Antilles island arc and adjacent backarc Grenada Basin. *Geochem., Geophys., Geosyst.*, 13:Q08007. doi:10.1029/2012GC004260
- Okada, H., and Bukry, D., 1980. Supplementary modification and introduction of code numbers to the low-latitude coccolith biostratigraphic zonation (Bukry, 1973; 1975). *Mar. Micropaleontol.*, 5:321–325. doi:10.1016/0377-8398(80)90016-X

Publication: 17 August 2013
MS 340-106

Figure F1. Site U1396 maps. A. Shaded image of topography-bathymetry, chaotic deposits (interpreted as debris avalanche deposits), and drill sites. (Continued on next page.)

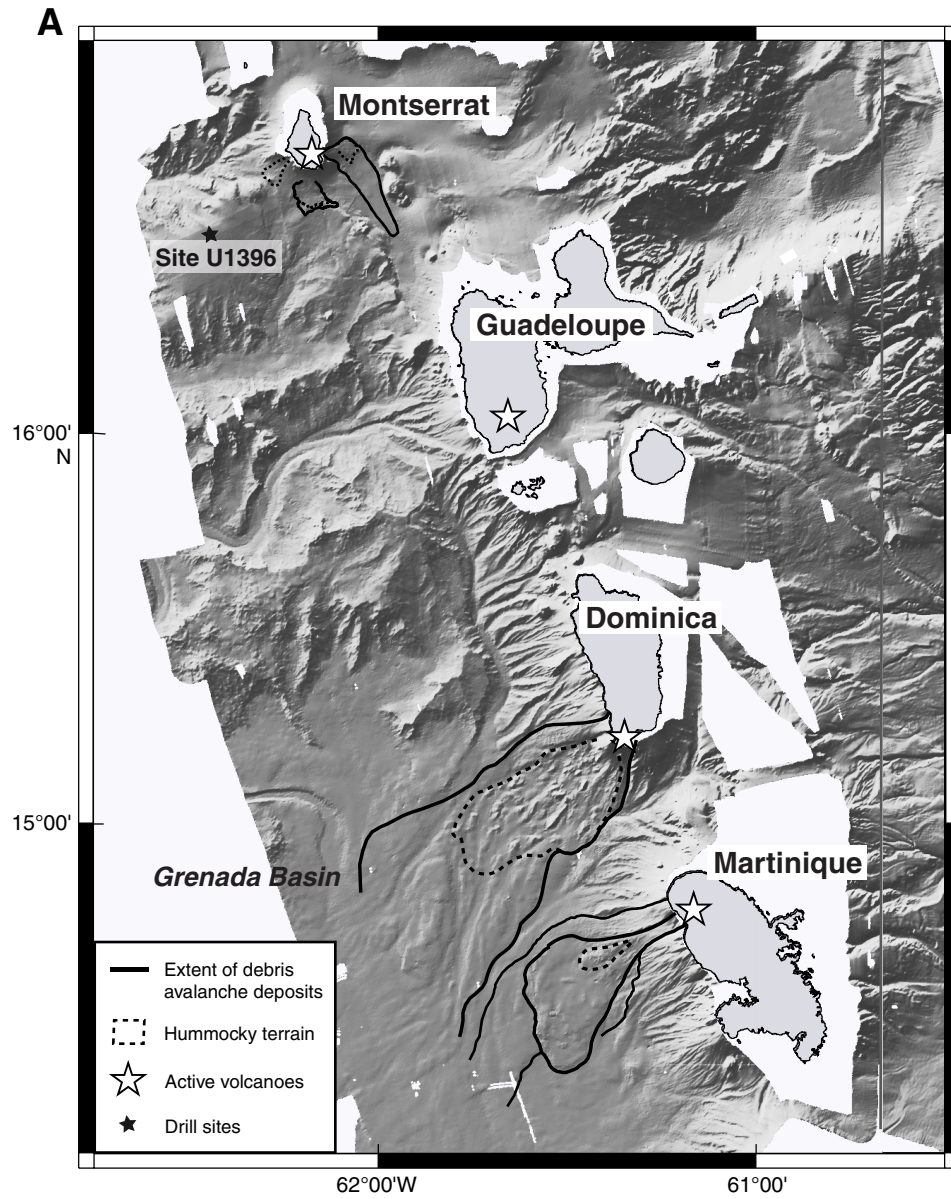


Figure F1 (continued). B. Location of seismic reflection lines, Site U1396. CDP = common depth point.

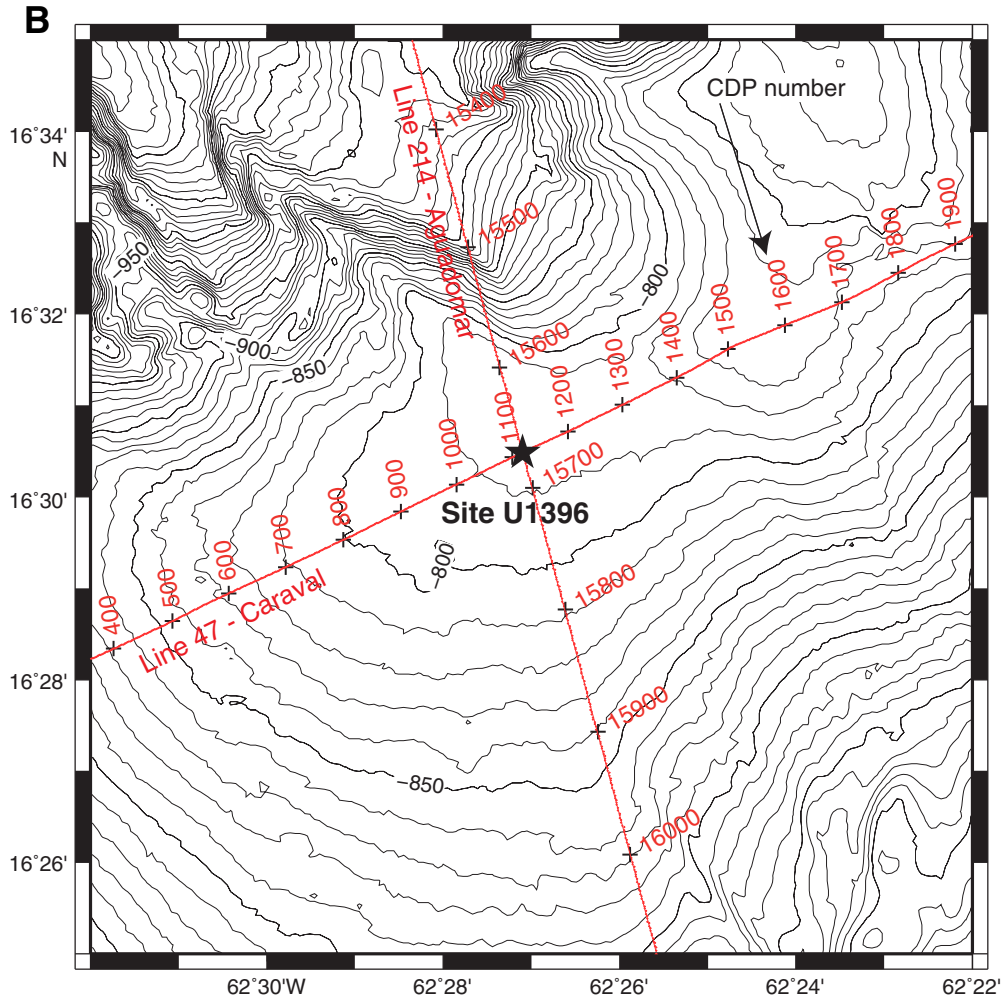


Figure F2. Distinct salmon pink pumice-rich deposit found in Holes U1396A and U1396C at 122–125 mbsf. Top of the section is at the left. Note the distinct normally graded units topped with a massive unsorted unit.

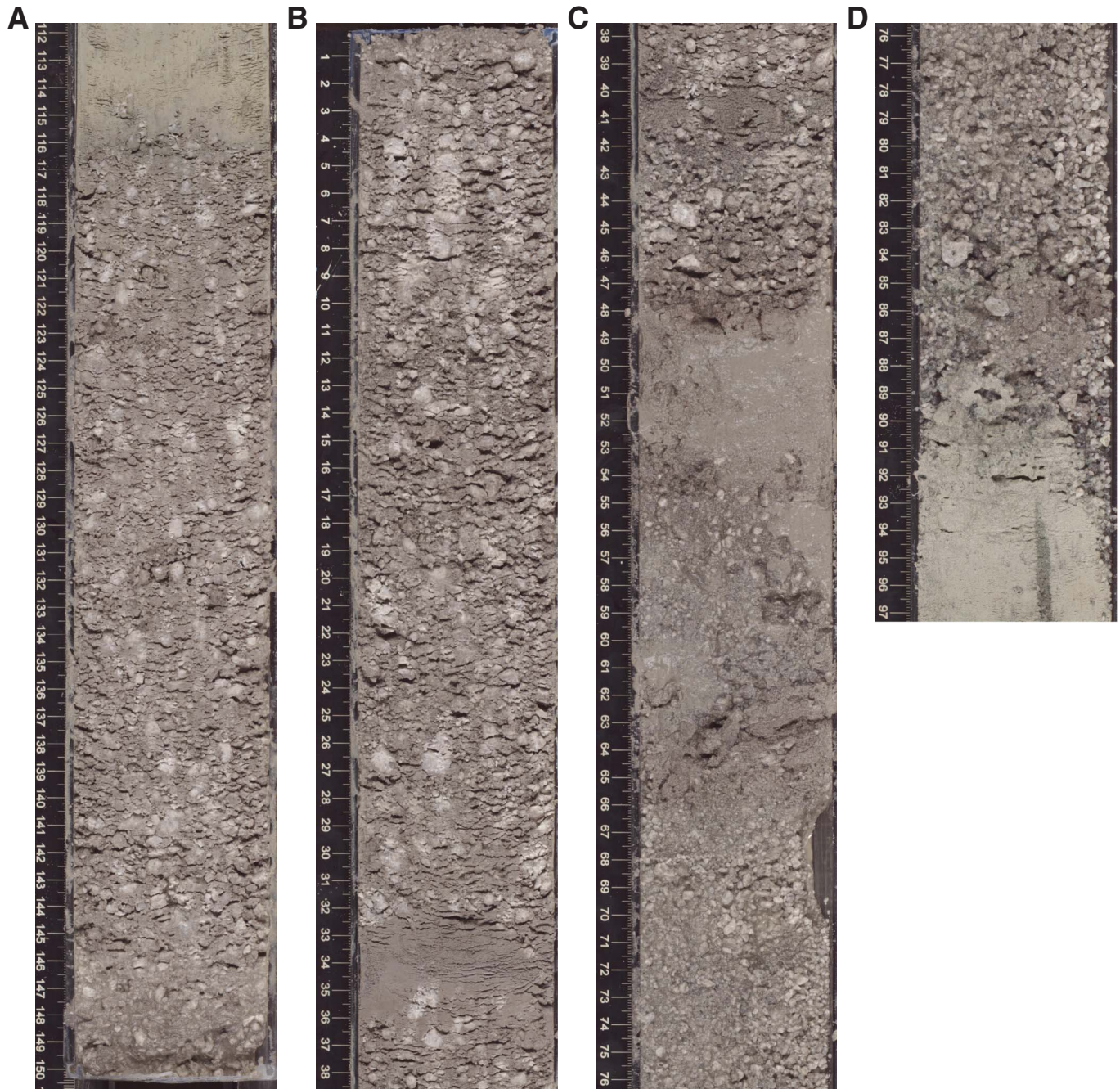


Figure F3. Integrated nannofossil and planktonic foraminiferal biozonation, Site U1396.

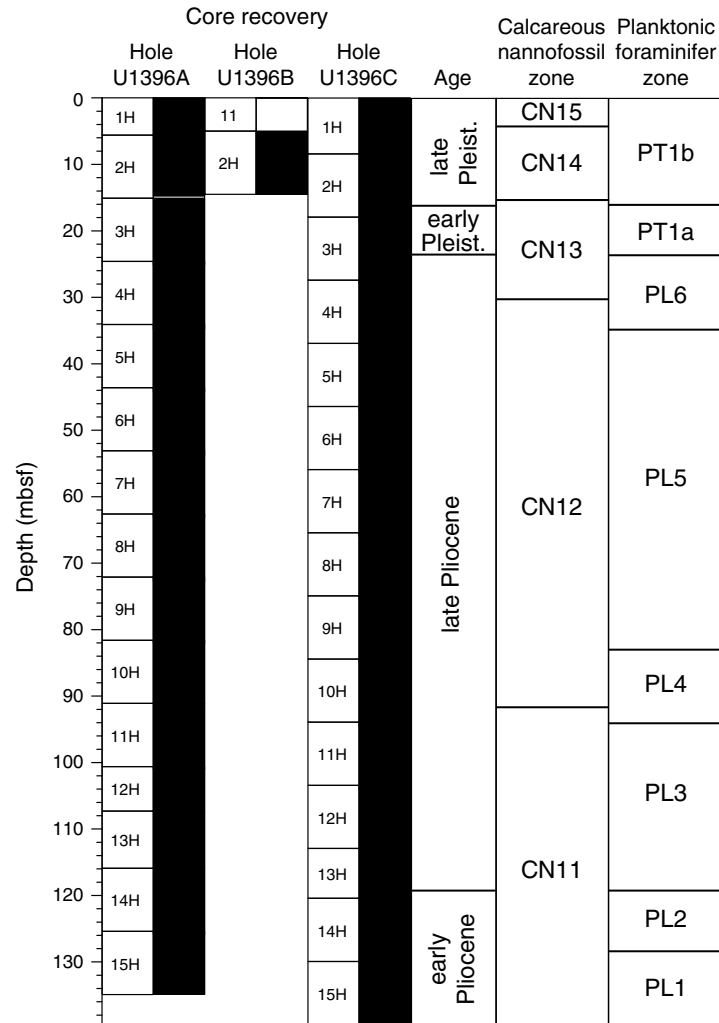




Figure F4. XRD patterns of selected samples from Hole U1396A. A. Sample 340-U1396A-9H-2, 119–120 cm. (Continued on next page.)

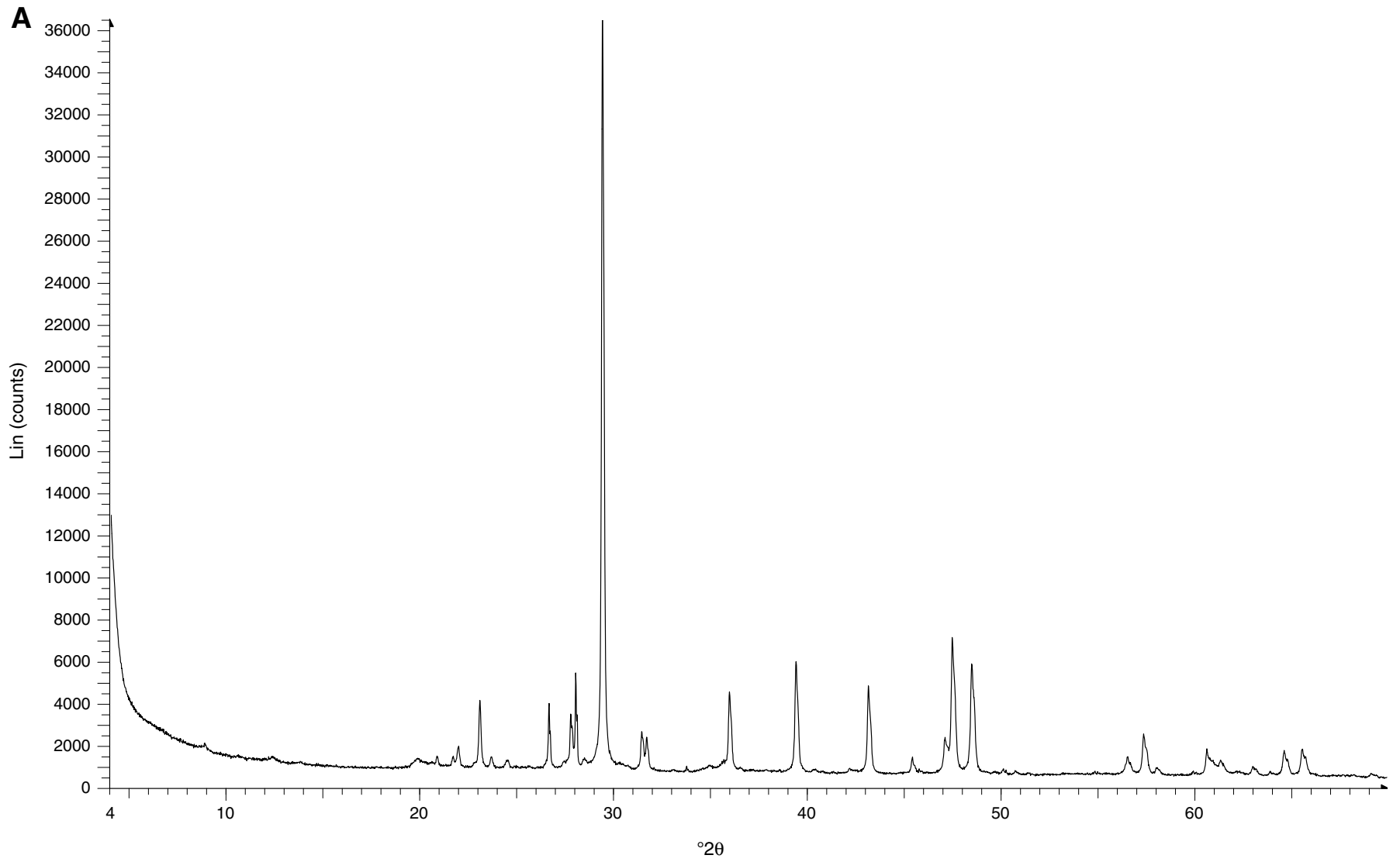




Figure F4 (continued). B. Sample 340-U1396A-12H-5, 26–27 cm.

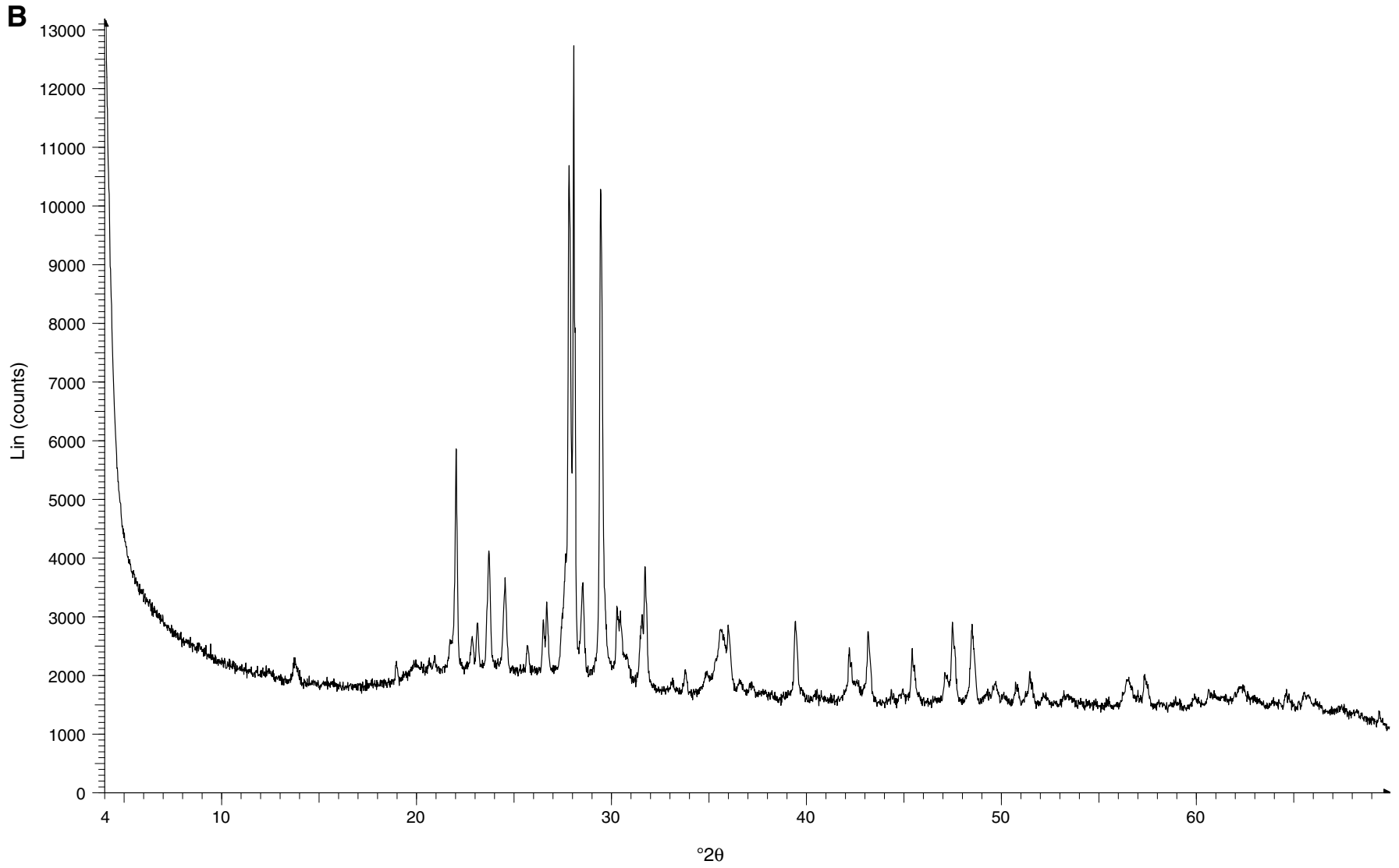


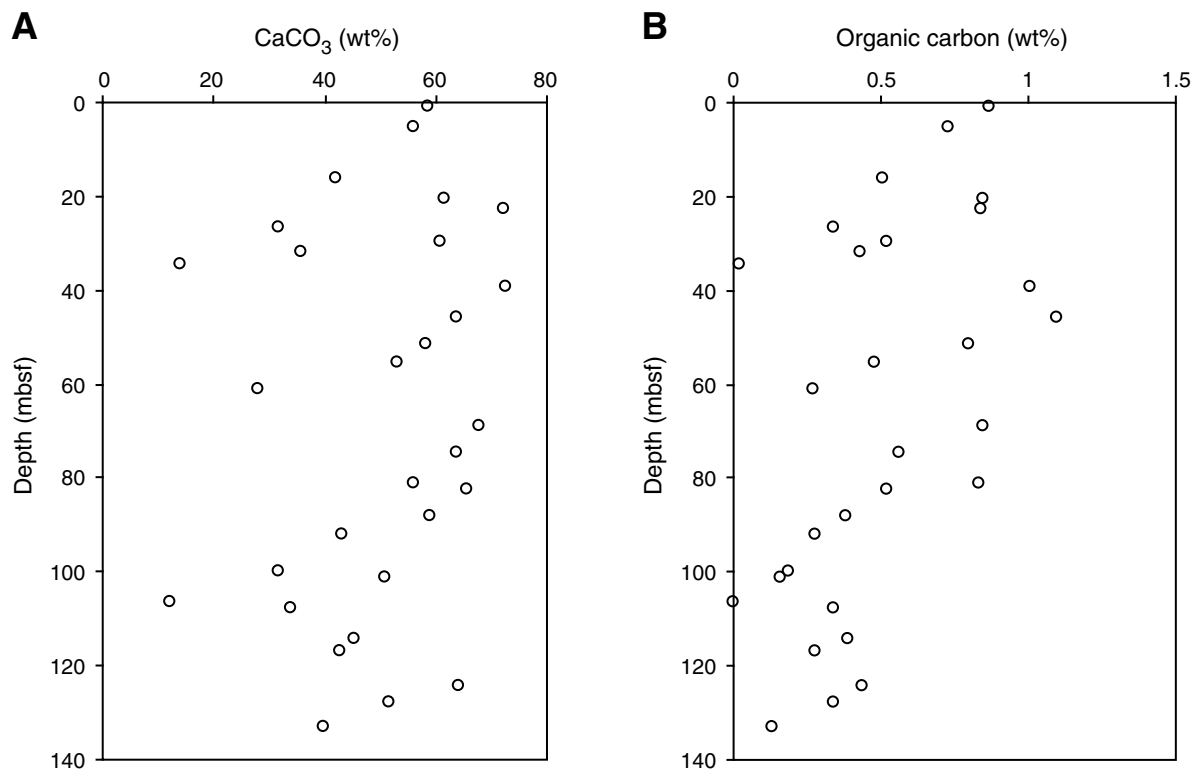
Figure F5. Solid-phase geochemical depth profiles, Site U1396. A. CaCO_3 . B. Organic carbon.



Figure F6. Pore water geochemical depth profiles, Hole U1396C. A. Alkalinity. B. NH₄⁺. C. Ca. D. Mg. E. K.

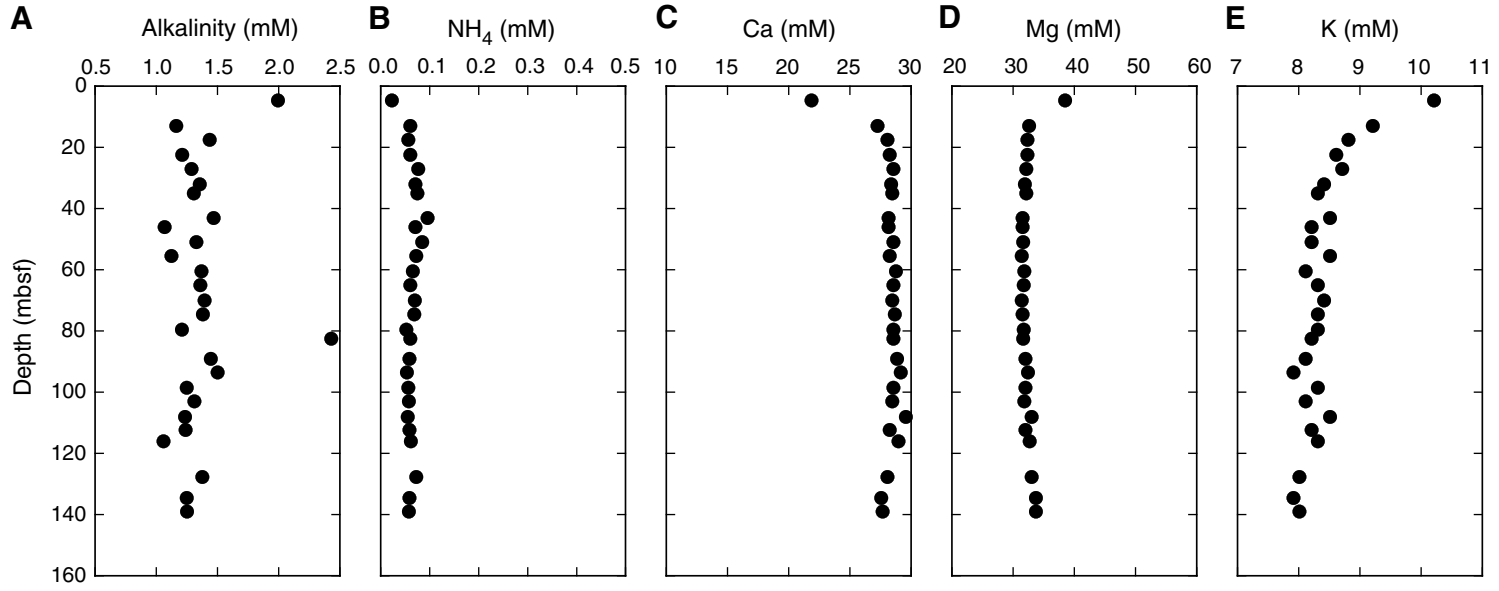




Figure F7. Magnetic susceptibility correlation of upper cores (0–50 mbsf), Holes U1396A (red) and U1396B (blue) to Hole U1396C (black). Magnetic susceptibility was measured on the Whole-Round Multisensor Logger (WRMSL). Negative values in the last column indicate a downhole shift.

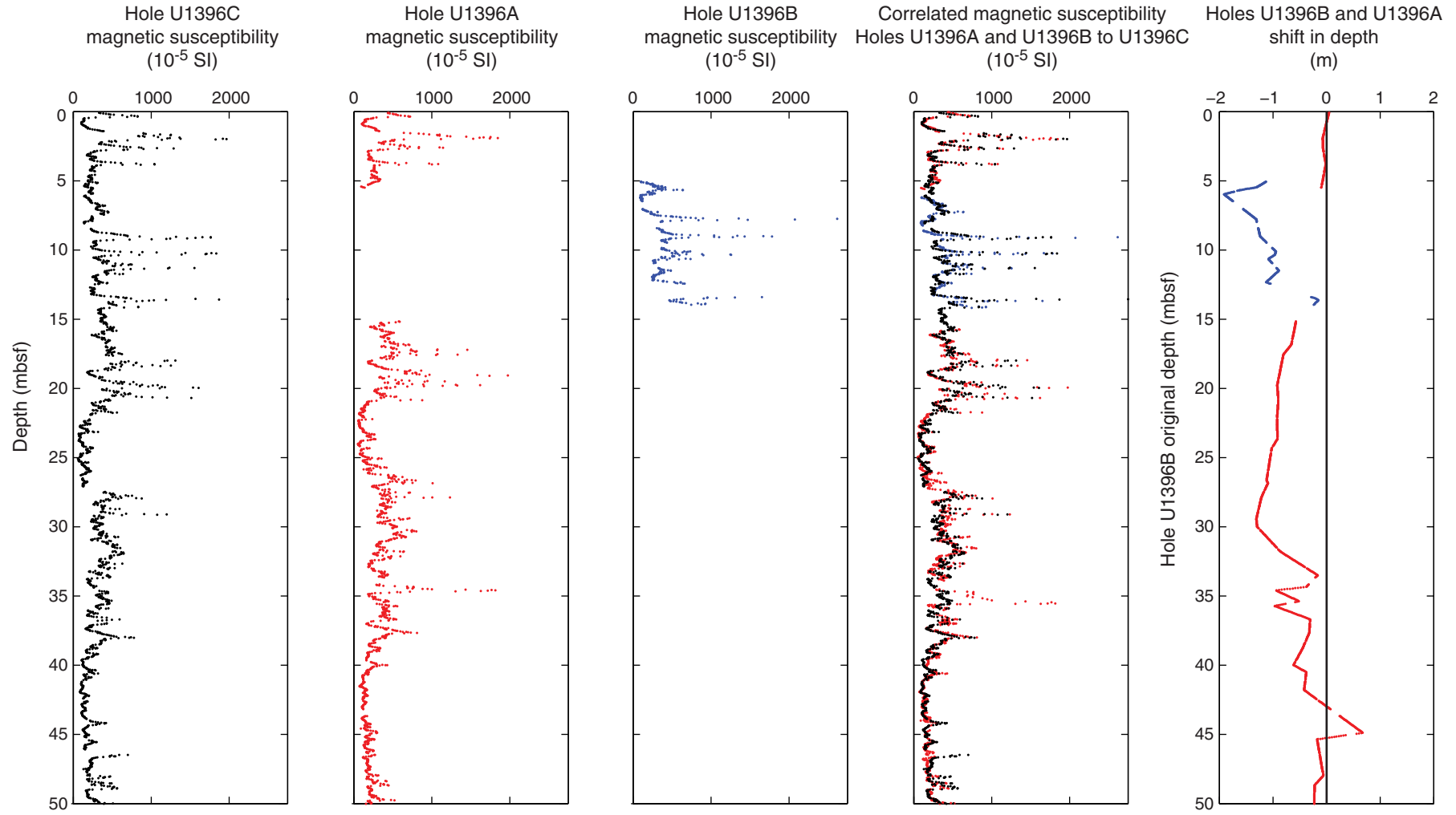




Figure F8. Magnetic susceptibility correlation of lower cores (50–140 mbsf), Hole U1396A (red) to Hole U1396C (black). Magnetic susceptibility was measured on the Whole-Round Multisensor Logger (WRMSL). Negative values in the last column indicate a downhole shift.

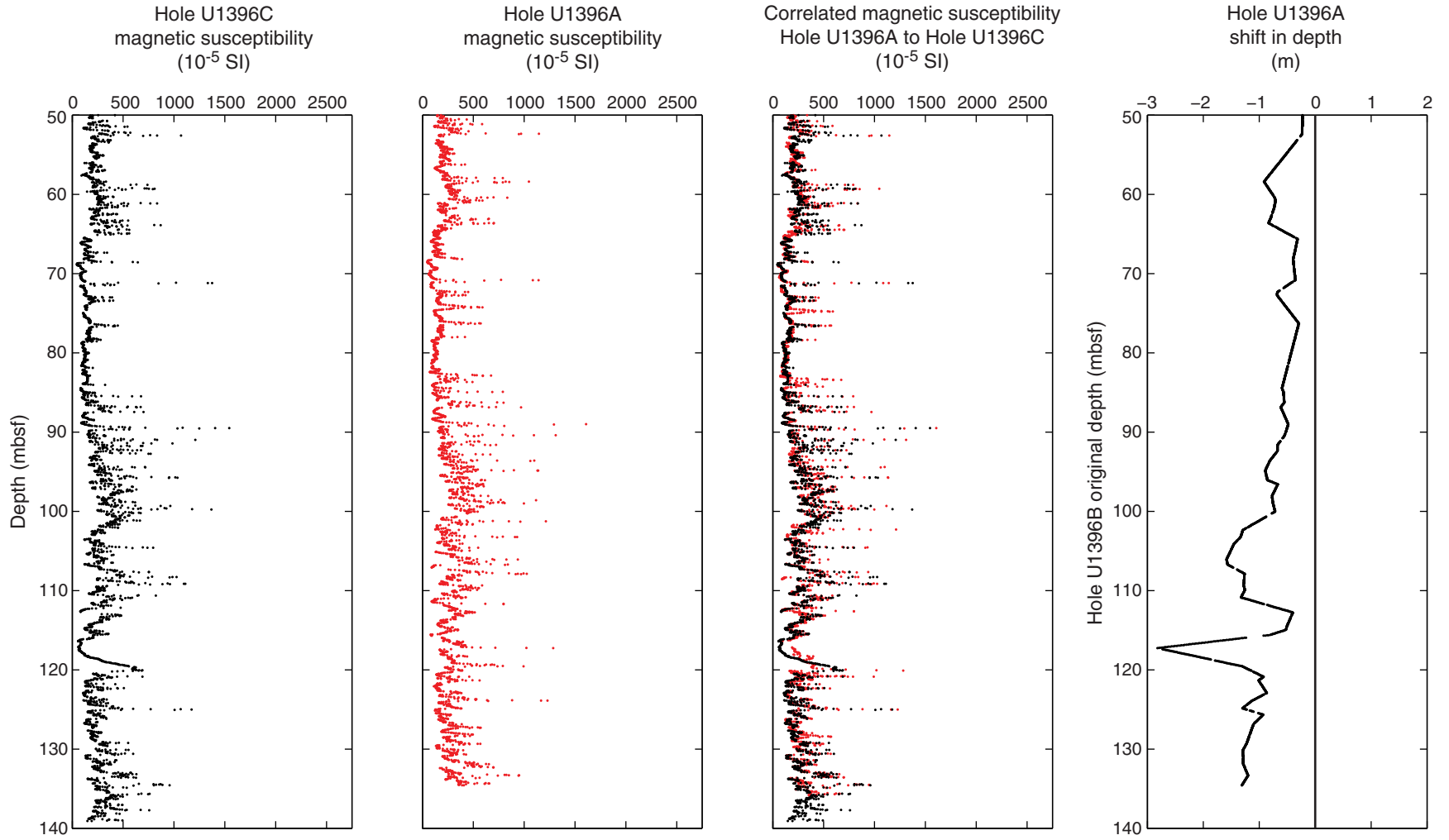




Figure F9. Physical properties, Holes U1396A (red), U1396B (green), and U1396C (blue). Whole-core data was excluded at both extremities of each core section to avoid core liner disturbances. Whole-Round Multisensor Logger (WRMSL) *P*-wave velocities were truncated when below 1500 m/s, corresponding to velocity in water. Discrete point measurements are shown with larger symbols. Vertical dashed line in the shear strength plot shows the maximum value that can be measured with the handheld penetrometer (220 kPa). AVS = automated vane shear.

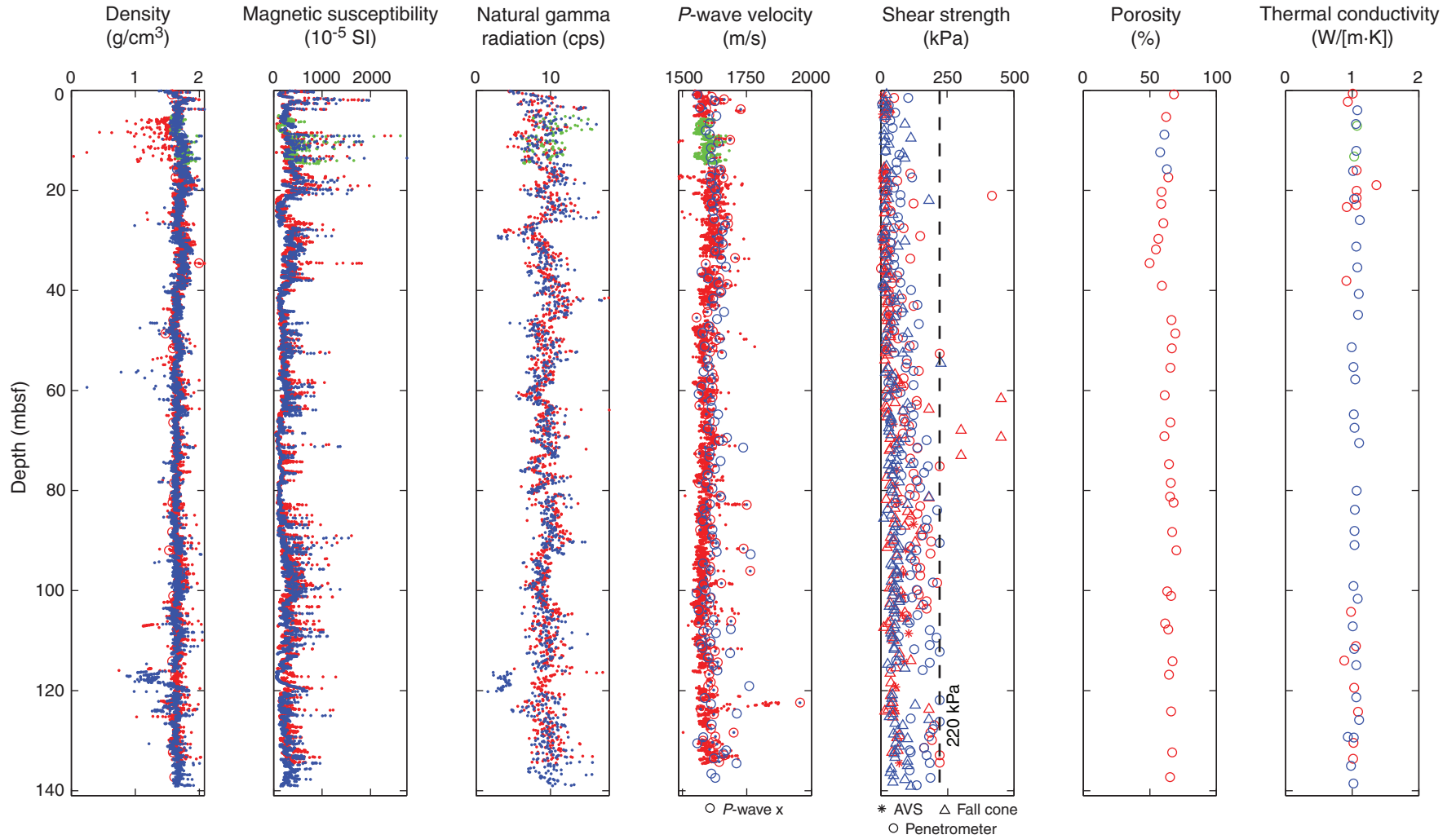


Figure F10. Temperature as a function of depth, Holes U1396A (blue) and U1396C (green). Straight line is a best fit to the measurements.

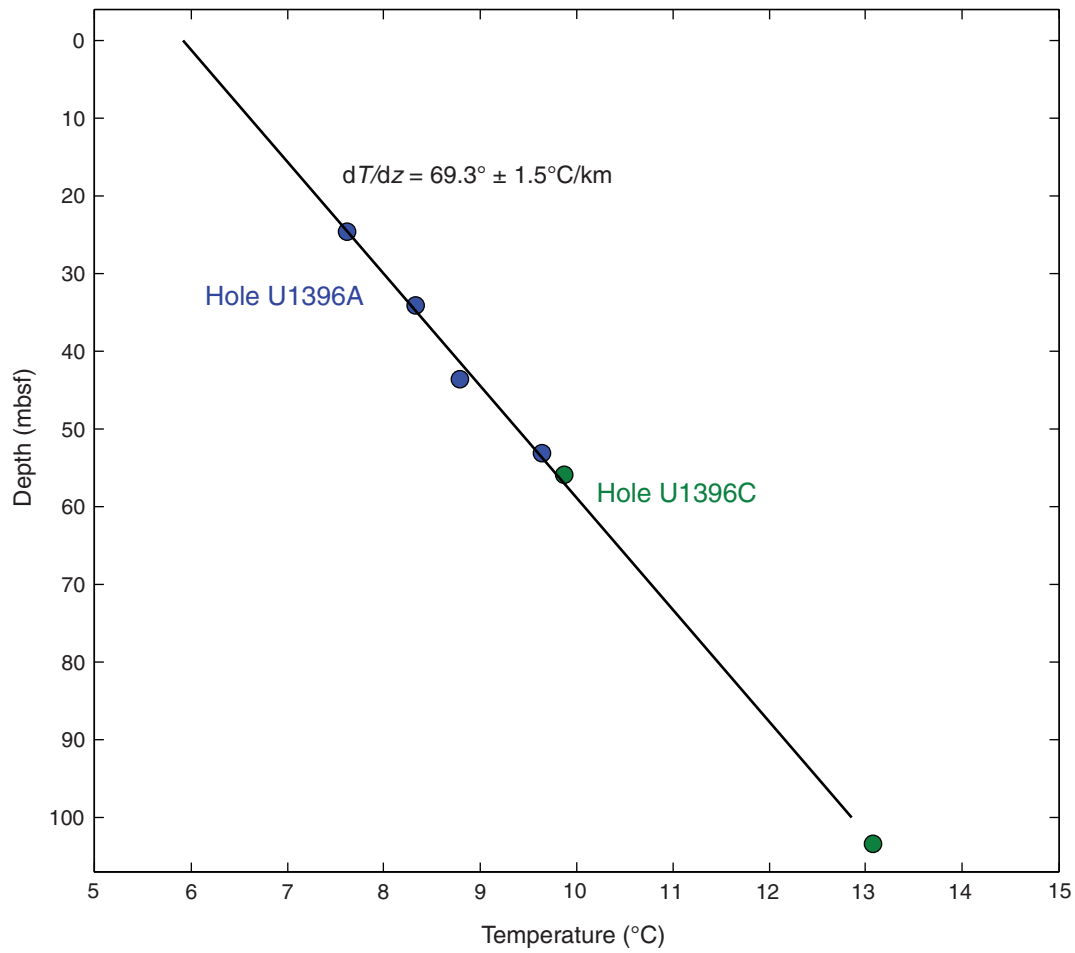


Figure F11. Plots of intensity of NRM_0 (red) and NRM_{20} (blue) and inclination and declination after 20 mT demagnetization, Holes U1396A and U1396B. Hole U1396B data (purple) is shown spliced into the Hole U1396A record. For directional data, red points show measurements made on cores recovered with nonmagnetic barrels and orange points denote the use of standard steel barrels. All red declination points are FlexIt tool-corrected to true north for the site $-15.6^\circ W$; orange points are discrete inclination guided data (see text). Black squares are discrete inclination measurements shown against a geocentric axial dipole (GAD) inclination of 30.6° . The black and white “barcode” illustrates periods of normal (black) and reversed polarity (white) with calibrated ages from the GPTS of Cande and Kent (1995).

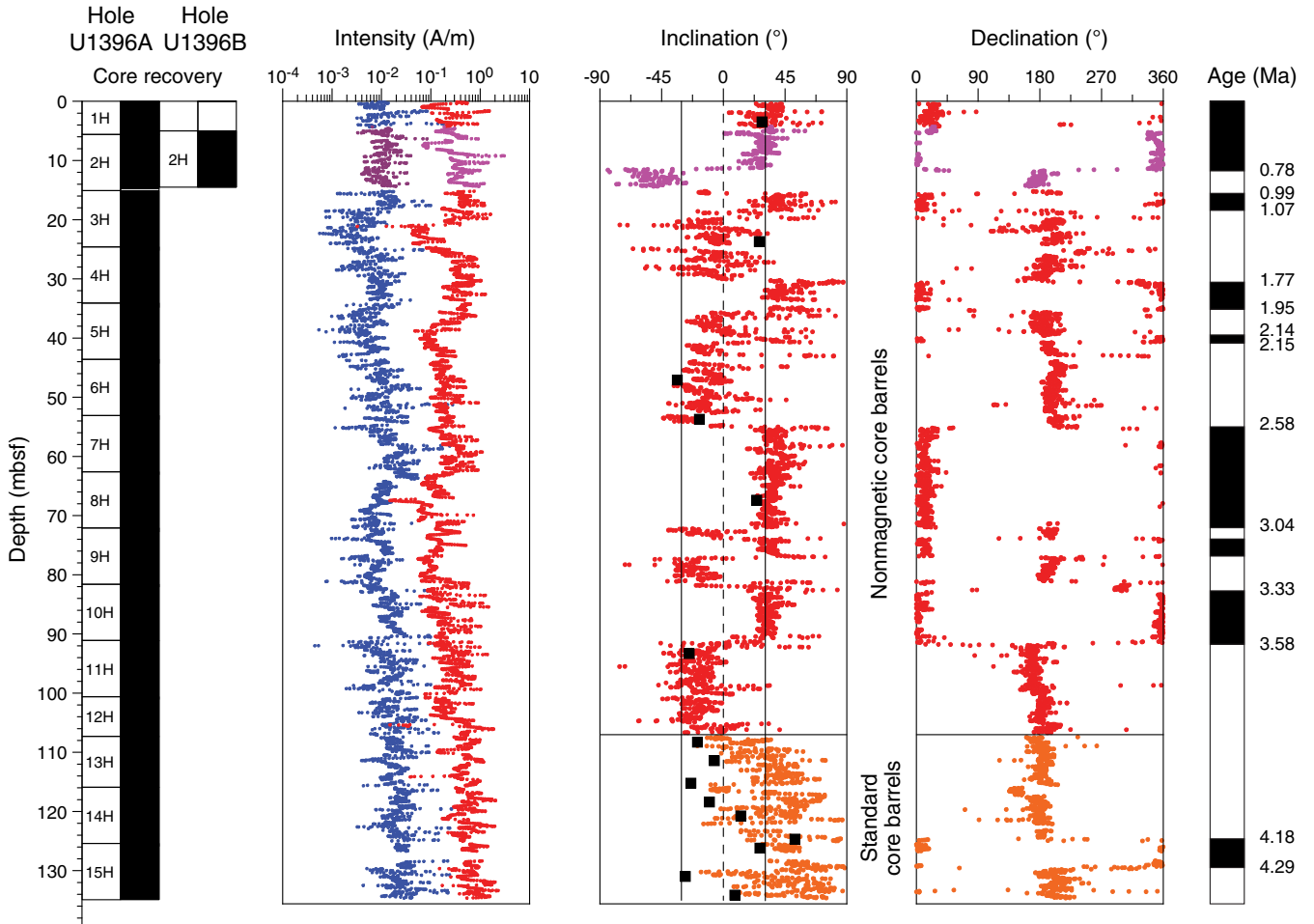


Figure F12. Plots of intensity of NRM_0 (red) and NRM_{20} (blue) and inclination and declination after 20 mT demagnetization, Hole U1396C. All declination points are FlexIt tool-corrected to true north for the site -15.6°W . Black squares are discrete inclination measurements shown against a geocentric axial dipole (GAD) inclination of 30.6° . The black and white “barcode” illustrates periods of normal (black) and reversed polarity (white) with calibrated ages from the GPTS of Cande and Kent (1995).

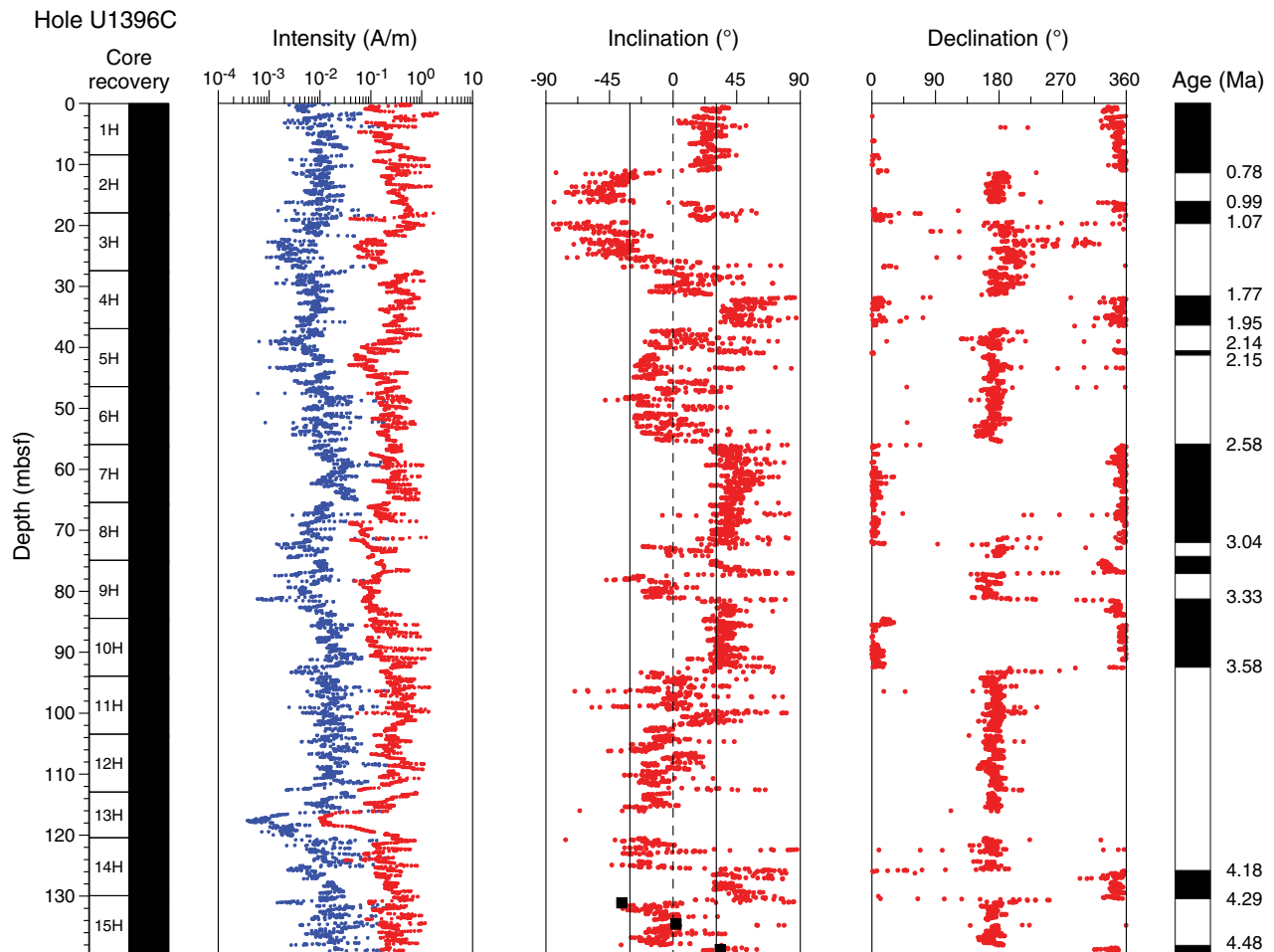


Figure F13. Magnetic susceptibility correlations used to transfer Hole U1396A depths onto Hole U1396C depths. The composite inclination record is shown on Hole U1396C.

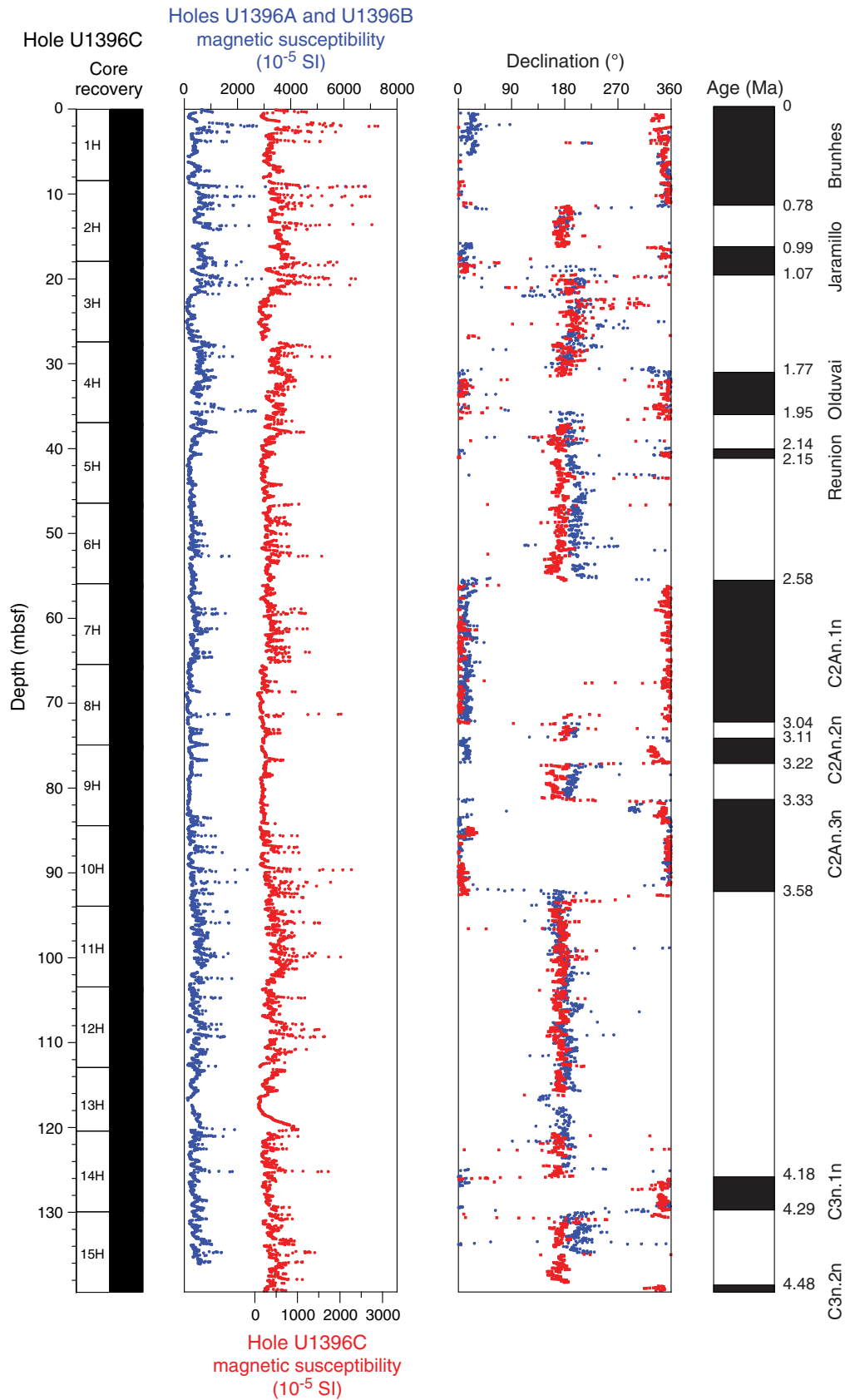


Figure F14. Age vs. depth, Hole U1396C. Reversal horizons are shown on the y-axis barcode diagram vs. the GPTS of Cande and Kent (1995) on the x-axis. Paleomagnetic directions compare well with biostratigraphic datums, which are split into nannofossil and planktonic foraminiferal datums.

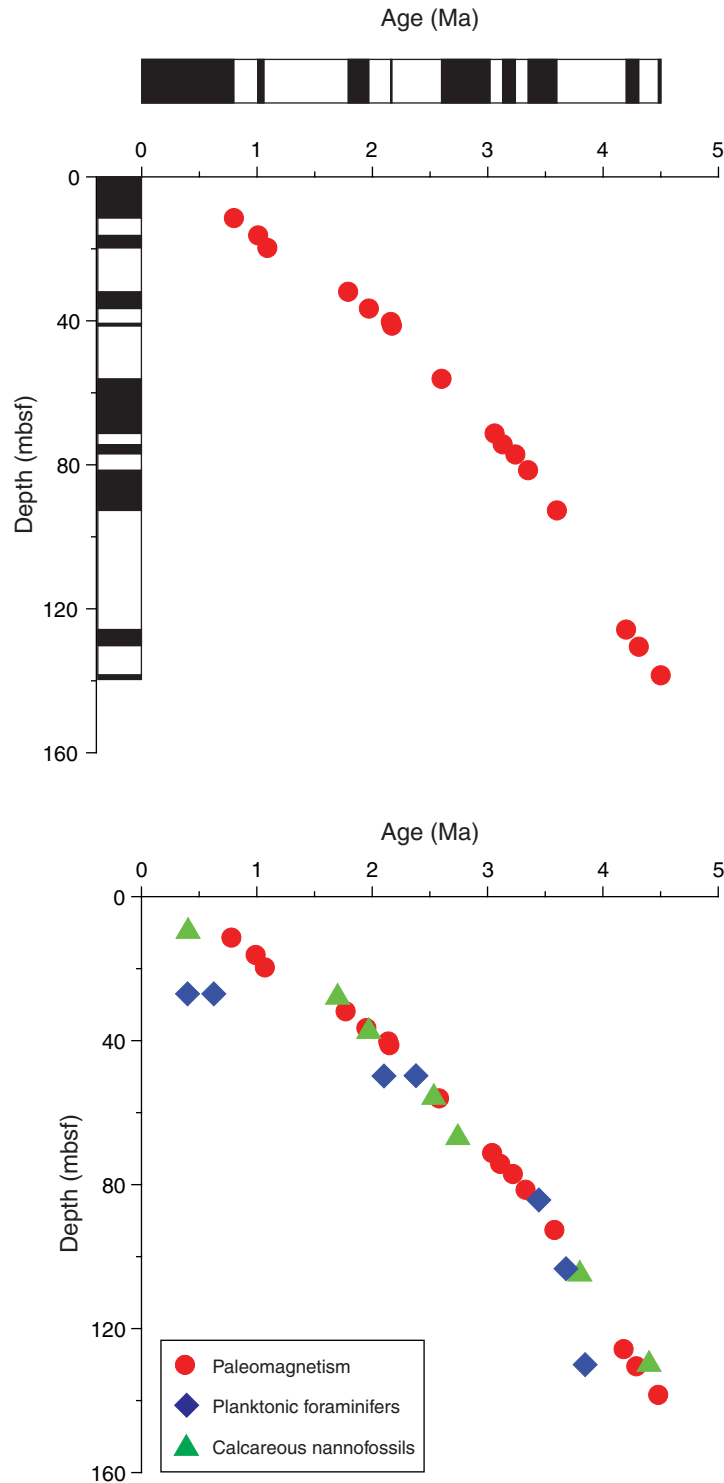


Table T1. Coring summary, Site U1396. (Continued on next page.)

Hole:	U1396A									
Latitude:	16°30.4841'N									
Longitude:	62°27.1017'W									
Water depth (m):	787.4									
Date started (UTC*):	1845 h 16 March 2012									
Date finished (UTC*):	1215 h 17 March 2012									
Time on hole (days):	0.7									
Seafloor depth DRF (m):	798.9									
Penetration DSF (m):	134.9									
Cored interval (m):	134.9									
Recovered length (m):	140.51									
Recovery (%):	104									
Total cores (no.):	15									
Hole:	U1396B									
Latitude:	16°30.4847'N									
Longitude:	62°27.0912'W									
Water depth (m):	787.4									
Date started (UTC*):	1215 h 17 March 2012									
Date finished (UTC*):	1330 h 17 March 2012									
Time on hole (days):	0.01									
Seafloor depth DRF (m):	798.9									
Penetration DSF (m):	14.5									
Cored interval (m):	9.5									
Recovered length (m):	10									
Recovery (%):	105									
Drilled interval (m):	5									
Drilled interval (no.):	1									
Total cores (no.):	1									
Hole:	U1396C									
Latitude:	16°30.4729'N									
Longitude:	62°27.0905'W									
Water depth (m):	786.6									
Date started (UTC*):	1330 h 17 March 2012									
Date finished (UTC*):	0530 h 18 March 2012									
Time on hole (days):	0.47									
Seafloor depth DRF (m):	798.1									
Penetration DSF (m):	139.4									
Cored interval (m):	139.4									
Recovered length (m):	145.92									
Recovery (%):	105									
Total cores (no.):	15									
Core	Top depth drilled DSF (m)	Bottom depth drilled DSF (m)	Advanced (m)	Recovered length (m)	Curated length (m)	Top depth cored CSF (m)	Bottom depth recovered CSF (m)	Recovery (%)	Time on deck (UTC*)	
340-U1396A-										
1H	0.0	5.6	5.6	5.63	5.63	0.0	5.63	101	3/17/12 07:45	
2H	5.6	15.1	9.5	9.17	9.17	5.6	14.77	97	3/17/12 08:40	
3H	15.1	24.6	9.5	10.08	10.08	15.1	25.18	106	3/17/12 09:35	
4H	24.6	34.1	9.5	10.23	10.23	24.6	34.83	108	3/17/12 10:25	
5H	34.1	43.6	9.5	10.17	10.17	34.1	44.27	107	3/17/12 11:15	
6H	43.6	53.1	9.5	10.17	10.17	43.6	53.77	107	3/17/12 12:05	
7H	53.1	62.6	9.5	9.96	9.96	53.1	63.06	105	3/17/12 12:40	
8H	62.6	72.1	9.5	10.14	10.14	62.6	72.74	107	3/17/12 13:15	
9H	72.1	81.6	9.5	9.96	9.96	72.1	82.06	105	3/17/12 13:50	
10H	81.6	91.1	9.5	9.58	9.58	81.6	91.18	101	3/17/12 14:25	
11H	91.1	100.6	9.5	9.94	9.94	91.1	101.04	105	3/17/12 14:55	
12H	100.6	107.3	6.7	6.78	6.78	100.6	107.38	101	3/17/12 15:40	
13H	107.3	115.9	8.6	8.65	8.65	107.3	115.95	101	3/17/12 16:45	
14H	115.9	125.4	9.5	9.98	9.98	115.9	125.88	105	3/17/12 17:35	
15H	125.4	134.9	9.5	10.07	10.07	125.4	135.47	106	3/17/12 18:20	
340-U1396B-										
11				*****Drilled from 0 to 5.0 mbsf*****						3/17/12 21:05
2H	5.0	14.5	9.5	10.00	10.00	5.0	15.00	105	3/17/12 21:20	
340-U1396C-										
1H	0.0	8.4	8.4	8.39	8.39	0.0	8.39	100	3/17/12 22:15	
2H	8.4	17.9	9.5	10.07	10.07	8.4	18.47	106	3/17/12 23:05	
3H	17.9	27.4	9.5	10.02	10.02	17.9	27.92	105	3/17/12 23:45	
4H	27.4	36.9	9.5	9.95	9.95	27.4	37.35	105	3/18/12 00:20	

Table T1 (continued).

Core	Top depth drilled DSF (m)	Bottom depth drilled DSF (m)	Advanced (m)	Recovered length (m)	Curated length (m)	Top depth cored CSF (m)	Bottom depth recovered CSF (m)	Recovery (%)	Time on deck (UTC*)
5H	36.9	46.4	9.5	10.11	10.11	36.9	47.01	106	3/18/12 00:50
6H	46.4	55.9	9.5	10.03	10.03	46.4	56.43	106	3/18/12 01:55
7H	55.9	65.4	9.5	10.11	10.11	55.9	66.01	106	3/18/12 02:25
8H	65.4	74.9	9.5	10.07	10.07	65.4	75.47	106	3/18/12 03:00
9H	74.9	84.4	9.5	9.98	9.98	74.9	84.88	105	3/18/12 03:35
10H	84.4	93.9	9.5	10.09	10.09	84.4	94.49	106	3/18/12 04:15
11H	93.9	103.4	9.5	10.15	10.15	93.9	104.05	107	3/18/12 05:50
12H	103.4	112.9	9.5	9.57	9.57	103.4	112.97	101	3/18/12 07:15
13H	112.9	120.4	7.5	7.59	7.59	112.9	120.49	101	3/18/12 07:50
14H	120.4	129.9	9.5	9.68	9.68	120.4	130.08	102	3/18/12 08:50
15H	129.9	139.4	9.5	10.11	10.11	129.9	140.01	106	3/18/12 09:25
Totals:			288.8	296.43	296.43				

* = ship local time was Universal Time Coordinated (UTC) – 4 h. DRF = drilling depth below rig floor, DSF = drilling depth below seafloor, CSF = core depth below seafloor. H = advanced piston corer.

Table T2. Solid-phase geochemistry, Site U1396.

Core, section	Depth (mbsf)		Carbon (wt%)				Nitrogen (wt%)
	Top	Bottom	CaCO ₃	Inorganic	Total	Organic	
340-U1396A-							
1H-1	0.77	0.78	58.79	7.05	7.92	0.87	BD
1H-4	5.28	5.29	56.17	6.74	7.46	0.73	BD
3H-1	16.30	16.31	42.08	5.05	5.56	0.51	BD
3H-4	20.60	20.61	61.40	7.36	8.21	0.85	BD
3H-6	23.16	23.17	72.32	8.67	9.51	0.84	0.04
4H-2	26.73	26.74	31.84	3.82	4.16	0.34	BD
4H-4	30.05	30.06	60.97	7.31	7.83	0.52	BD
4H-6	32.34	32.35	35.64	4.27	4.70	0.43	BD
5H-1	34.61	34.62	14.08	1.69	1.71	0.02	BD
5H-4	39.47	39.48	72.57	8.70	9.71	1.01	BD
6H-2	46.07	46.08	63.87	7.66	8.76	1.10	0.01
6H-6	52.12	52.13	58.12	6.97	7.77	0.80	0.01
7H-2	55.49	55.50	53.17	6.38	6.86	0.48	0.01
7H-6	61.29	61.30	28.19	3.38	3.65	0.27	BD
8H-5	69.52	69.53	67.84	8.13	8.98	0.85	0.01
9H-2	74.81	74.82	63.91	7.66	8.22	0.56	0.06
9H-7	81.64	81.65	56.11	6.73	7.56	0.83	0.02
10H-1	82.41	82.42	65.68	7.87	8.39	0.52	0.02
10H-5	88.30	88.31	58.84	7.06	7.44	0.38	0.03
11H-1	91.93	91.94	43.13	5.17	5.45	0.28	0.02
11H-7	100.49	100.50	31.61	3.79	3.98	0.19	0.01
12H-1	101.04	101.05	50.98	6.11	6.27	0.16	0.02
12H-5	106.62	106.63	12.27	1.47	1.47	BD	0.01
13H-1	107.77	107.78	33.97	4.07	4.41	0.34	0.02
13H-5	114.15	114.16	45.38	5.44	5.83	0.39	0.02
14H-1	116.85	116.86	42.87	5.14	5.42	0.28	0.01
14H-6	124.54	124.55	63.98	7.67	8.11	0.44	0.02
15H-2	127.95	127.96	51.46	6.17	6.51	0.34	0.02
15H-6	133.25	133.26	39.97	4.79	4.92	0.13	0.01
340-U1396C-							
2H-3	12.51	12.52	49.91	5.98	6.14	0.16	0.01

BD = below detection, values reported as 0.

Table T3. Composition of interstitial pore water, Hole U1396C.

Core, section	Depth (mbsf)		Alkalinity (mM)	pH	Cl (mM)	±	Salinity	NH ₄ (mM)	Na (mM)	±	Mg (mM)	±	K (mM)	±	Ca (mM)	±	ΣS (mM)	±
	Top	Bottom																
340-U1396C-																		
1H-3	4.40	4.50	1.99	7.40	567.5		37	0.02	483.4	9.3	38.4	0.6	10.2	0.1	21.8	0.4	27.4	0.6
2H-3	12.80	12.90	1.16	7.26	574.2		37	0.06	488.5	1.5	32.5	0.3	9.2	0.1	27.2	0.1	27.2	0.2
2H-6	17.30	17.40	1.43	7.25	576.1		37	0.06	488.7	2.1	32.2	0.3	8.8	0.2	28.0	0.1	27.2	0.2
3H-3	22.20	22.30	1.21	7.16	574.4		37	0.06	490.9	3.8	32.2	0.3	8.6	0.2	28.2	0.2	27.2	0.2
3H-6	26.80	26.90	1.28	7.13	579.4		37	0.08	498.2	9.7	32.0	0.8	8.7	0.2	28.5	0.6	26.6	0.4
4H-3	31.80	31.90	1.35	7.16	575.9		37	0.07	490.8	2.6	31.8	0.3	8.4	0.3	28.3	0.2	26.9	0.2
4H-5	34.80	34.90	1.30	7.26	577.5		37	0.07	492.1	4.3	32.0	0.3	8.3	0.0	28.4	0.3	26.8	0.1
5H-4	42.80	42.90	1.46	7.55	576.0		38	0.09	491.3	2.4	31.4	0.3	8.5	0.3	28.1	0.1	26.7	0.2
5H-6	45.80	45.90	1.06	6.86	579.0		37	0.07	485.6	3.4	31.4	0.3	8.2	0.3	28.1	0.2	26.7	0.3
6H-3	50.70	50.80	1.32	7.57	579.0		37	0.08	486.8	4.3	31.5	0.5	8.2	0.3	28.5	0.2	26.7	0.3
6H-6	55.30	55.40	1.12	7.25	580.8		38	0.07	484.7	3.2	31.3	0.3	8.5	0.2	28.2	0.2	26.6	0.2
7H-3	60.30	60.40	1.36	7.20	576.9		38	0.06	486.7	1.5	31.7	0.3	8.1	0.1	28.7	0.1	26.7	0.3
7H-6	64.80	64.90	1.35	7.28	580.0		38	0.06	486.8	3.2	31.6	0.3	8.3	0.2	28.5	0.3	26.7	0.3
8H-3	69.80	69.90	1.39	7.66	578.6		37	0.07	488.0	2.1	31.3	0.3	8.4	0.3	28.4	0.1	26.6	0.3
8H-6	74.35	74.45	1.37	7.80	578.4		38	0.07	491.1	2.1	31.4	0.2	8.3	0.0	28.6	0.0	26.4	0.3
9H-3	79.30	79.40	1.20	7.32	578.4		37	0.05	486.6	2.1	31.6	0.3	8.3	0.1	28.5	0.1	26.6	0.2
9H-5	82.30	82.40	2.42	7.45	575.8		38	0.06	488.0	2.8	31.5	0.3	8.2	0.2	28.5	0.2	26.7	0.3
10H-3	88.82	88.92	1.44	7.48	576.6		37	0.06	489.4	3.1	31.9	0.3	8.1	0.3	28.8	0.2	26.9	0.2
10H-6	93.35	93.45	1.50	7.23	576.2		37	0.05	492.5	3.0	32.3	0.4	7.9	0.1	29.1	0.3	27.0	0.4
11H-3	98.30	98.40	1.24	7.12	578.7		37	0.06	491.3	5.3	31.9	0.5	8.3	0.1	28.5	0.3	26.8	0.2
11H-6	102.71	102.81	1.31	7.36	576.5		38	0.06	487.1	3.6	31.7	0.3	8.1	0.1	28.4	0.2	26.4	0.3
12H-3	107.83	107.93	1.23	7.38	576.7		38	0.05	502.5	0.5	32.9	0.5	8.5	0.2	29.5	0.2	27.5	0.9
12H-6	112.10	112.20	1.23	7.47	576.8		37	0.06	487.7	1.6	31.9	0.3	8.2	0.2	28.2	0.1	26.8	0.3
13H-2	115.81	115.91	1.05	7.31	575.9		37	0.06	494.7	5.9	32.6	0.2	8.3	0.2	28.9	0.3	26.9	0.0
14H-5	127.49	127.59	1.37	7.33	576.2		37	0.07	488.3	3.4	32.9	0.3	8.0	0.5	28.0	0.1	27.0	0.2
15H-3	134.33	134.43	1.24	7.23	572.6	0.7	38	0.06	484.7	2.8	33.6	0.4	7.9	0.2	27.5	0.3	27.2	0.2
15H-6	138.80	138.90	1.25	7.41	573.3	0.1	37	0.06	489.5	11.7	33.6	0.2	8.0	0.3	27.6	0.5	27.0	0.0

Uncertainties for Cl represent $\pm 1\sigma$ based on repeat analyses. Shaded samples represent average values for Na, Mg, K, Ca, and ΣS (total sulfur) from duplicate analyses from separate runs. Samples in italics represent averages from within-run duplicates.

Table T4. Correlation of Hole U1396A to Hole U1396C.

Hole U1396A depth (mbsf)	Hole U1396C depth (mbsf)	Difference (m)	Hole U1396A depth (mbsf)	Hole U1396C depth (mbsf)	Difference (m)
0.362	0.335	-0.027	72.336	73.011	0.675
1.929	2.002	0.072	72.730	73.413	0.683
2.604	2.673	0.069	76.293	76.585	0.293
3.779	3.793	0.014	84.469	85.062	0.594
15.568	16.159	0.592	84.933	85.500	0.567
16.841	17.499	0.658	86.274	86.826	0.552
17.548	18.354	0.806	86.853	87.469	0.616
19.070	19.953	0.884	89.012	89.493	0.480
19.770	20.690	0.921	90.423	90.969	0.546
20.845	21.745	0.900	91.635	92.309	0.674
22.211	23.137	0.926	92.425	93.102	0.678
23.641	24.555	0.915	93.618	94.428	0.811
24.324	25.348	1.024	94.861	95.755	0.893
26.635	27.754	1.119	96.064	96.917	0.853
26.851	27.945	1.094	96.591	97.259	0.667
27.535	28.714	1.179	98.059	98.831	0.772
27.889	29.107	1.218	99.007	99.761	0.754
29.416	30.726	1.310	100.030	100.745	0.716
29.989	31.286	1.297	102.369	103.663	1.294
31.800	32.659	0.859	103.241	104.574	1.333
33.495	33.660	0.166	104.077	105.528	1.451
34.331	34.705	0.373	106.079	107.664	1.585
34.594	35.539	0.945	106.713	108.279	1.566
35.375	35.886	0.510	107.863	109.127	1.264
35.712	36.687	0.975	109.351	110.631	1.280
36.683	36.988	0.305	109.921	111.178	1.257
37.667	37.991	0.324	110.863	112.190	1.327
38.755	39.199	0.444	112.761	113.161	0.399
39.986	40.603	0.617	114.630	115.143	0.513
40.496	40.875	0.379	114.947	115.471	0.525
41.793	42.211	0.418	115.598	116.401	0.803
44.884	44.207	-0.677	117.258	120.079	2.822
45.348	45.525	0.177	119.554	120.858	1.305
47.976	48.036	0.060	120.895	121.816	0.921
48.685	48.911	0.226	121.336	122.349	1.013
52.364	52.594	0.230	122.920	123.785	0.864
57.935	58.797	0.862	123.889	125.015	1.126
58.417	59.330	0.913	124.849	126.150	1.301
60.410	61.135	0.725	125.659	126.588	0.929
60.775	61.484	0.709	126.839	127.941	1.102
61.740	62.475	0.735	129.351	130.580	1.229
63.096	63.897	0.801	130.135	131.428	1.293
63.631	64.464	0.834	131.907	133.191	1.284
65.633	65.948	0.315	133.335	134.535	1.200
68.167	68.559	0.392	134.349	135.639	1.290
70.829	71.184	0.356			

Table T5. Correlation of Hole U1396B to Hole U1396C.

Hole U1396B depth (mbsf)	Hole U1396C depth (mbsf)	Difference (m)
5.208	6.400	1.192
5.389	6.659	1.270
5.475	6.789	1.314
5.665	7.273	1.608
5.971	7.886	1.915
7.771	9.084	1.313
9.010	10.250	1.241
10.111	11.055	0.944
10.342	11.307	0.965
10.647	11.733	1.087
11.489	12.378	0.889
12.332	13.461	1.129
13.488	13.703	0.215
13.620	13.768	0.148
13.898	14.123	0.225

Table T6. Samples measured for paleomagnetism, Site U1396.

Core	Measured (mT)	APC core barrel
340-U1396A-		
1H	0, 10, 20	Nonmagnetic
2H	No, liner shattered	Nonmagnetic
3H	0, 10, 20	Nonmagnetic
4H	0, 10, 20	Nonmagnetic
5H	0, 10, 20	Nonmagnetic
6H	0, 10, 20	Nonmagnetic
7H	0, 10, 20	Nonmagnetic
8H	0, 10, 20	Nonmagnetic
9H	0, 10, 20	Nonmagnetic
10H	0, 10, 20	Nonmagnetic
11H	0, 10, 20	Nonmagnetic
12H	0, 10, 20	Nonmagnetic
13H	0, 10, 20	Standard
14H	0, 10, 20	Standard
15H	0, 10, 20	Standard
340-U1396B-		
2H	0, 10, 20	Nonmagnetic
340-U1396C-		
1H	0, 10, 20	Nonmagnetic
2H	0, 10, 20	Nonmagnetic
3H	0, 10, 20	Nonmagnetic
4H	0, 10, 20	Nonmagnetic
5H	0, 10, 20	Nonmagnetic
6H	0, 10, 20	Nonmagnetic
7H	0, 10, 20	Nonmagnetic
8H	0, 10, 20	Nonmagnetic
9H	0, 10, 20	Nonmagnetic
10H	0, 10, 20	Nonmagnetic
11H	0, 10, 20	Nonmagnetic
12H	0, 10, 20	Nonmagnetic
13H	0, 10, 20	Nonmagnetic
14H	0, 10, 20	Nonmagnetic
15H	0, 10, 20	Nonmagnetic

APC = advanced piston corer.